whole small intestines by tracing the outline of the areas with an image processing program, Image J (National Institutes of Health, Bethesda, MD).

RNA extraction

Mice were sacrificed and the dissected small intestines were used for the preparation of total RNA. Each of the frozen samples was homogenized in a 1 ml/0.1 g tissue of TRI REAGENT (Sigma-Aldrich Japan, Tokyo, Japan) with a POLYTRON tissue homogenizer (Kinematica, Littau-Lucerne, Switzerland) and incubated for 10 min at room temperature. A conventional chloroform extraction and isopropanol/ethanol precipitate technique were used to isolate RNA.

Microarray analysis

Total RNA was re-purified by RNeasy spin columns (Qiagen, Valencia, CA) according to the manufacturer's instructions. All samples were monitored using an Agilent Bioanalyzer (Agilent Biotechnologies, Boeblingen, Germany) and consistently demonstrated high-quality RNA (28S/18S ratio, ~2). GeneChip analysis using an MG-U74Av2 array (Affymetrix, Santa Clara, CA) was performed according to the Affymetrix protocol. Data were analyzed using the Affymetrix Microarray Suite (MAS) v.5.0 with all of the parameters set at default values (a global normalization was applied). Probe sets that had three present A MAS detection calls per group (3 samples) in at least one of the groups were included in the analysis.

MetaGene Profiler and Cell Illustrator Online

MetaGene Profiler has been developed to evaluate the significance of predefined sets of genes from transcriptome data (http://metagp.ism.ac.jp/) [11]. The method accumulates statistical evidence from a set of genes in order to build a more powerful test than can be achieved by analyzing individual genes. In the present study, we first predefined the group of genes for each gene ontology (GO) term [all three categories, i.e., biological process (BP), cellular component (CC) and molecular function (MF), were used]. The number of gene sets annotated by GO terms was over 20,000. To obtain the *P*-values for individual genes, Welch's *t* test was performed. The individual *P*-values of the genes included in the gene set were integrated to obtain "the integrated *P*-value for the gene set", as described previously (http://metagp.ism.ac.jp/). A gene set containing too small a number of genes is, in principle, unsuitable for evaluation of over-represented gene sets. Preliminary examination suggested GO terms containing more than 100 genes provided relatively little information because these terms represent too broad a concept to give a foothold for further biological investigation. Therefore MGP analysis was applied to the gene sets consisting of 4–99 genes. As described in the results section, the above-mentioned analysis suggested a possible involvement of the adenosine system in the pathogenesis of IND-induced enteropathy and its amelioration by OGT. Therefore additional analysis using MGP was performed on the gene sets representing distinct facets of the adenosine system, that is, purine metabolism, adenosine metabolism and/or signaling, three types of adenosine-related apoptosis and literature analysis of ADA. CIO is a graphic platform for modeling and simulating signaling pathways (http://www.cellillustrator.com) [12].

Real-time RT-PCR

Real time RT-PCR was performed in two laboratory sites where different PCR methodologies were used: the TaqMan® Gold RT-PCR Kit without controls (Applied Biosystems, Foster City, CA), and the QuantiFast™ SYBR Green PCR kit (Qiagen) according to the manufacturer's instructions. These two assays gave essentially the same results. For TaqMan® assay, combinations of probes and primers of Mm01247822_m1 for ADA and Mm00607939_s1 for beta-actin were used. Real time PCR analysis was performed using an ABI Prism 7900HT (Applied Biosystems) with the following thermal cycling conditions: 1 cycle at 50°C for 2 min, 1 cycle at 95°C for 10 min, followed by 40 cycles at 95°C for 15 s and 60°C for 1 min. All samples were run in triplicate. Data was normalized against beta-actin. For the QuantiFast™ assay, the primers for ADA (forward: 5′-GAGCTGCGCAACATT ATCG-3′, reverse: 5′-GCCTTCATCTCCACAAACTC-3′) and GAPDH (forward: 5′-AGGAAGCTCACTGGCATG G-3′, reverse: 5′-CCTGCTTCACCACCTTCTTG-3′) were used. The cycle parameters involved an initial activation step at 95°C for 5 min, followed by 35 cycles of denaturation at 95°C for 10 s then annealing and extension at 60°C for 30 s. After amplification, samples were kept at 55°C for 1 min and the temperature was gradually raised by 0.5°C every 10 s to perform the melt-curve analysis. All procedures of real time PCR were performed on the iCycler iQ™ Real-Time PCR Detection System (Bio-Rad Laboratories, Tokyo, Japan) All reactions were performed in triplicate. The threshold cycles (Ct) were used to quantify the mRNA expression levels of samples using GAPDH for normalization.

In situ hybridization

In situ hybridization was performed at Genostaff Co., Ltd. Detailed protocols are described in Supplementary Materials.

Effects of adenosine receptor blockade on IND-induced enteropathy with OGT

We wanted to test the role of the adenosine system on the effect of OGT during IND-induced enteropathy. Thus, we examined the effect of adenosine receptor antagonists on the lethality induced by IND with or without OGT. An adenosine receptor A2a antagonist 8-(3-chlorostyryl) caffeine (CSC; 10 mg/kg) or an equal volume of vehicle were administered intraperitoneally (i.p.) for five consecutive days from one day before the first IND treatment.

Results

Effect of Orengedokuto on indomethacin-induced enteropathy

As previously reported [8], IND induced lethal small intestinal ulceration and OGT prevented the ulcerations and the lethality. OGT rescued mice from IND-induced death (Fig. 1a). OGT reduced the number and area of IND-induced ulcerations (Fig. 1b, c).

Gene expression in the murine small intestine

For the gene expression studies, the mice used for this experiment were divided into four groups: N (normal), I (IND-treated), N/O (OGT-treated) and I/O (IND- and OGT-treated). Preparation of tissue samples was performed 48 h after the first injection of IND when more than 90% of mice still survived even in group I. Three comparison sets were made, that is, EXP_IND: N versus I (effect of IND), EXP_OGT: N versus N/O (effect of OGT), EXP_OGT_IND: I versus I/O (effect of OGT in IND-enteropathy model), and *P*-value for each probe set was calculated by Welch's *t* test. A list of genes that displayed increased or decreased levels of expression in each comparison set is shown in Supplementary Table S1–S3. For nine genes, the changes in gene expression induced by IND were partially abrogated by OGT (highlighted in bold font in Table S1, S2). OGT decreased ADA expression both in EXP_OGT and EXP_OGT_IND (highlighted in bold font in Table S2, S3).

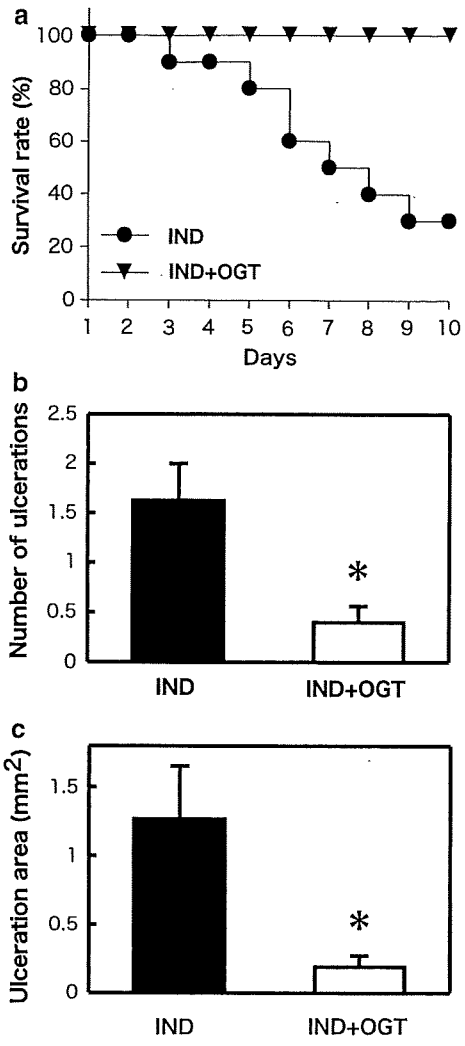

Fig. 1 **a** Orengedokuto (OGT) rescued mice from indomethacin (IND)-induced death. Survival curves were drawn using the Kaplan–Meier method. The difference in survival ratio at day 10 was analyzed by Fisher's exact test, $*P < 0.01$ ($n = 10$ per group) **b**, **c** OGT reduced IND-induced small intestinal lesions. Small intestines were harvested at 24 h after the second injection of IND. The number and areas of ulcerations were calculated macroscopically.$*P < 0.01$, data represent the means ± SEM ($n = 10$ per group)

Gene set analyses by MetaGene Profiler on GO terms

Filtering genes by setting the threshold for expression level, fold-changes, statistical significance, etc. is not ideal because the setting of the threshold cannot eliminate the problem of arbitrary selection. Furthermore, single-gene analysis has been known to have a number of major limitations. MGP, a recent developed method to evaluate microarray data at the level of gene sets, gives the "integrated *P*-value" for a given gene set by integrating *P*-values of all probe sets contained in the gene set. MGP facilitates an evaluation of the statistical significance of the given gene set. Initial analysis was performed using the

gene sets defined by the GO consortium. The "integrated *P*-values" for all possible gene sets defined by all GO terms (>20,000 terms) were calculated and the top 20 GO terms in MF, BP and cell component (CC) categories for EXP_IND are shown in Table 1 and Supplementary Table S4. A detailed discussion of these results is given in the Supplementary Materials. As shown in Table 1, among the GO terms denoting relatively broad and general concepts, those containing a small number of genes specific for particular biological activity, such as "rhodopsin-like receptor activity" and "ADA activity", were ranked. The gene list of "rhodopsin-like receptor activity" contains 4 probe sets for adenosine receptors among 19 probe sets in total. The results of MGP analysis for EXP_IND_OGT are shown in Table 2 and Supplementary Table S5. For the MF category, "deaminase activity" whose major members are ADAs, "rhodopsin-like receptor activity" and "ADA activity" were ranked. These MGP analyses prompted us to hypothesize a possible involvement of the adenosine system in the enteropathy and recovery by IND and OGT, respectively. Because the spectrum of adenosine functions is extremely wide, we defined several subsets of adenosine system-related genes. Further MGP analyses were then performed on the newly defined gene sets. This secondary MGP analyses suggested that the genes involved in adenosine metabolism were the most affected gene set by IND and/or OGT treatment (Table 3; details have been described in Supplementary Materials). MGP analysis for EXP_OGT gave only a few GO terms (7 GO terms in 3 categories with integrated *P*-value <0.05) suggesting that OGT has little or no effect on the expression profile of normal small intestines (data not shown).

Table 1 MGP analysis on EXP_IND: effect of IND

MF (molecular function)		
GO ID	GO term	Integrated P
0003779	Actin binding	1.48E-14
0008565	Protein transporter activity	1.65E-11
0004930	G-protein coupled receptor activity	2.40E-11
0004842	Ubiquitin-protein ligase activity	9.41E-11
0008234	Cysteine-type peptidase activity	1.76E-10
0003682	Chromatin binding	4.00E-10
0004197	Cysteine-type endopeptidase activity	5.36E-10
0030145	Manganese ion binding	1.33E-09
0005200	Structural constituent of cytoskeleton	1.98E-09
0008289	Lipid binding	5.90E-09
0005529	Sugar binding	1.76E-08
0046983	Protein dimerization activity	2.82E-08
0008026	ATP-dependent helicase activity	4.28E-08
0001584	*Rhodopsin-like receptor activity*	4.45E-08
0004000	*Adenosine deaminase activity*	5.04E-08
0030528	Transcription regulator activity	5.48E-08
0008083	Growth factor activity	5.65E-08
0004386	Helicase activity	5.93E-08
0042802	Identical protein binding	8.37E-08
0046982	Protein heterodimerization activity	1.24E-07

Biological investigation of a possible involvement of the adenosine system in the effects by IND and/or OGT

In the next step, the possible involvement of the adenosine system was examined biologically. Firstly, ISH was performed to clarify the localization of ADA, which was most clearly affected by IND/OGT treatment (Fig. 2). ADA expression was observed specifically at the luminal surface of intestinal villous tips. It was increased in IND-treated mice, which was reduced by co-treatment with OGT. ADA signals were absent in the site of ulceration or perforation where villi had been destroyed because of the exclusive localization of ADA to villous tips (data not shown). Next, we performed real time RT-PCR to confirm the change of ADA gene expression of the small intestine. In accordance with microarray and ISH data, IND increased the expression of ADA mRNA in the small intestine whereas OGT decreased the expression level of ADA mRNA (Fig. 3). Administration of OGT alone also decreased ADA mRNA (Fig. 3). To determine whether adenosine signaling is involved in the effects elicited by IND and/or OGT, we administered an adenosine A2a receptor antagonist, CSC, to IND-treated mice with or without OGT and observed lethality. Treatment with CSC alone gave no significant effect on IND-treated/untreated mice (data not shown) but abrogated the OGT's preventive effect on IND-induced enteropathy (Fig. 4).

Investigation of the active ingredients of OGT for IND-induced death

To gain an insight into the active ingredients responsible for OGT's beneficial effect, we prepared three fractions consisting mainly of (a) alkaloids, (b) high molecular weight substances (e.g. polysaccharides) or (c) the residues, whose contents were equivalent to those contained in 2% OGT. Mice treated with the alkaloid fraction survived IND-induced death. By contrast, the high molecular weight fraction and the residue fraction had no preventive effect and only a modest preventive effect, respectively (Fig. 5a). Therefore we next tested the effects of four major alkaloids contained in OGT on the lethality induced by IND. Diets containing each alkaloid at twice the concentration corresponding to that in 2% OGT (2%OGT includes 0.0703% berberine, 0.00706%

Table 2 MGP analysis on EXP_IND_OGT: effect of OGT in IND_enteropathy

MF (molecular function)		
GO ID	GO term	Integrated P
0003924	GTPase activity	2.94E-05
0046873	Metal ion transporter activity	6.23E-04
0019239	*Deaminase activity*	2.74E-03
0004445	Inositol-polyphosphate 5-phosphatase activity	3.05E-03
0004601	Peroxidase activity	5.46E-03
0004907	Interleukin receptor activity	6.01E-03
0003847	1-Alkyl-2-acetylglycerophosphocholine esterase activity	9.05E-03
0001584	*Rhodopsin-like receptor activity*	1.31E-02
0005044	Scavenger receptor activity	1.56E-02
0004252	Serine-type endopeptidase activity	1.68E-02
0004000	*Adenosine deaminase activity*	1.81E-02
0043022	Ribosome binding	1.89E-02
0004930	G-protein coupled receptor activity	2.10E-02
0016772	Transferase activity, transferring phosphorus-containing groups	2.34E-02
0003779	Actin binding	2.39E-02
0005375	Copper ion transporter activity	2.47E-02
0005385	Zinc ion transporter activity	2.52E-02
0005200	Structural constituent of cytoskeleton	2.76E-02
0000049	tRNA binding	2.96E-02
0004263	Chymotrypsin activity	3.12E-02

Table 3 MGP analysis on selected gene sets of adenosine system

Gene set	Description	Effect of IND	Effect of OGT in IND-model	Effect of OGT
1	Purine metabolism	2.896E-02	1.019E-02	9.341E-01
2	Adenosine metabolism	1.935E-06	1.860E-02	6.567E-01
3	Adenosine signaling	2.977E-02	2.829E-01	8.654E-01
4	Adenosine metabolism/signaling	1.307E-05	5.245E-02	8.718E-01
5	T cell apoptosis subset	3.513E-01	4.211E-02	7.906E-01
6	Other cell apoptosis subset	1.824E-04	6.813E-03	9.530E-01
7	AdoHcy-mediated apoptosis	6.306E-01	1.630E-01	9.086E-01
8	Literature analysis	1.182E-07	8.794E-07	5.397E-01

Definition of gene sets (Table S6 in supplementary material)

coptisine, 0.00129% palmatine and 0.00176% magnoflorine) were administered from the first injection of IND until 10 days after the first IND injection ($n = 10$ per group). Our results showed that berberine and coptisine, but not palmatine and magnoflorine, possibly reduced the incidence of IND-induced death (data not shown). Then we focused our attention on berberine, which has been ethically used. Berberine suppressed IND-induced lethality in a dose-dependent manner (Fig. 5b). Real time RT-PCR showed that berberine treatment reduced IND-induced increase in ADA mRNA expression in the small intestine (Fig. 6).

Schematic representation of changes in gene expression of adenosine system by CIO (http://www.cellillustrator.com)

We represent the changes in gene expression of the adenosine system by a visualization method using CIO (Fig. 7). The genes involved in the adenosine system were classified into three categories; intracellular adenosine metabolism, extracellular adenosine metabolism and adenosine signal transduction. Intracellular adenosine is provided by SAH hydrolase (Ahcy) from *S*-adenosylhomocysteine and degraded by ADA or adenosine kinase (ADK). In the

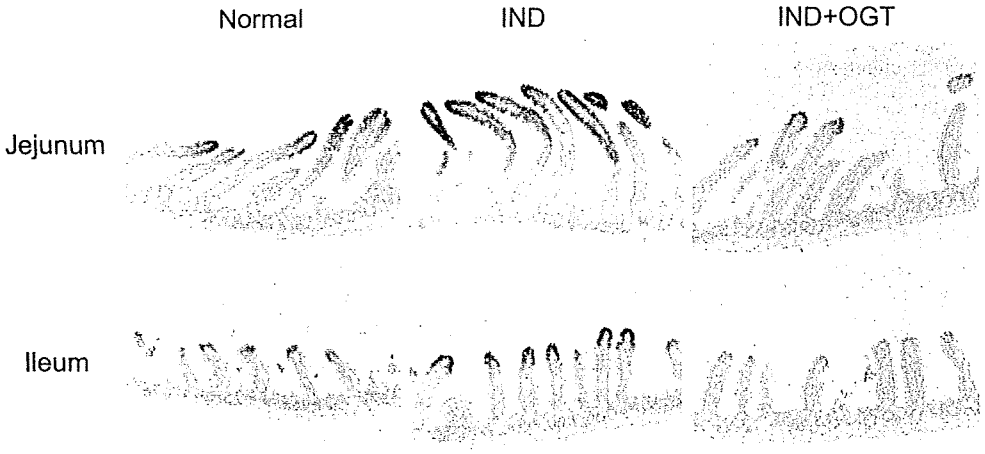

Fig. 2 In situ hybridization for ADA mRNA. Small intestines were harvested 24 h after the second injection of IND

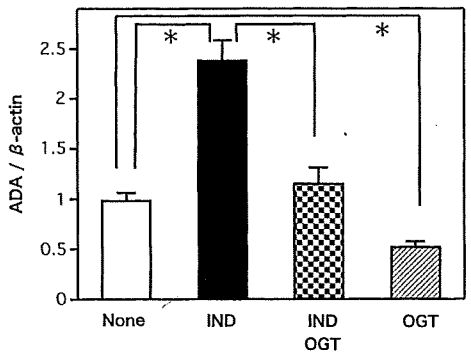

Fig. 3 OGT reduced ADA mRNA expression in the small intestines of both IND-treated and untreated mice. Small intestines were harvested at 24 h after the second injection of IND. $^*P < 0.05$, t test with Bonferroni correction. Data represent the means ± SEM ($n = 3$–5 per group)

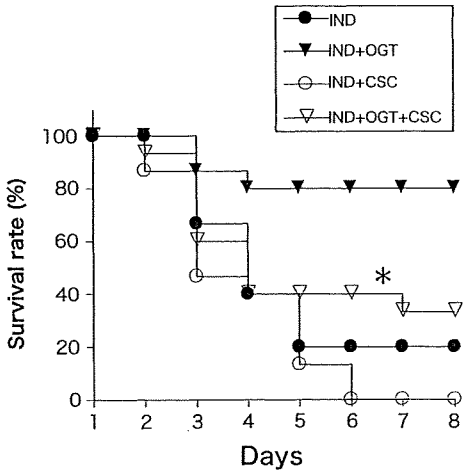

Fig. 4 Adenosine A2a receptor antagonist abrogates the effect of OGT. Adenosine A2a receptor antagonist (CSC; 10 mg/kg i.p.) was injected for 5 consecutive days prior to the first injection of IND. Survival curves were drawn using the Kaplan–Meier method and statistical analysis was done by the logrank test. $^*P < 0.02$ versus IND + OGT ($n = 15$ per group)

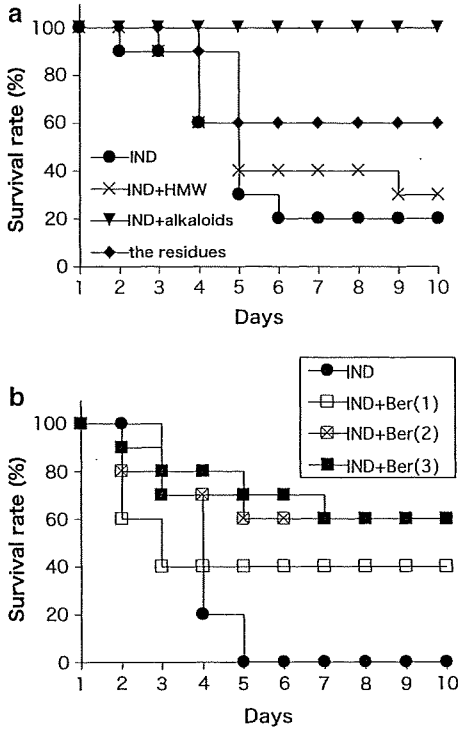

Fig. 5 **a** Effect of OGT fractions on IND-induced lethality. Diets containing each fraction at the concentration relevant to that in 2%OGT were administered from the first injection of IND until the end of the experiments. HMW: high molecular weight fraction. The alkaloid fraction had the strongest protective effect. Survival curves were drawn using the Kaplan–Meier method ($n = 10$ per group). **b** Berberine suppressed IND-induced lethality in a dose-dependent manner. Diets containing berberine at 1× [Ber(1)], 2× [Ber(2)] or 3× [Ber(3)] concentration corresponding to that in 2% OGT were administered from the first IND injection until the end of the experiment. Survival curves were drawn using the Kaplan–Meier method ($n = 10$ per group)

inflammatory state, large amounts of extracellular adenosine are produced from ATP via the successive conversion by CD73/ectonucleotidase (Nt5e) and CD39 (Entpd2) and degraded by ectopically expressed ADA. Extracellular

adenosine binds to adenosine receptors (A2a, A2b) and transduces signals to MAPK1 and 3 through relevant G proteins (Gna11, Gnai2, Gnai3, Gnao1 and Gnas3). HIF1A is a master transcription factor which regulates the large portion of genes involved in the adenosine system. The expression of other relevant genes such as endonucleotidase (Nt5c2), nucleotide transporters (Slc28 family and Slc29 family), adenosine A1 and A3 receptors (Adora1, Adora3) were not detected nor assessed in the present study. The fold change and *P*-value for each gene provided by GeneChip analysis are represented as the size of icon and the line thickness of the wraparound frame, respectively. The figure clearly shows IND predominantly activates gene expression involved in extracellular adenosine metabolism. This suggests that in IND-treated small intestines a large amount of adenosine is synthesized and then degraded resulting in activation of the adenosine signal transduction pathway. OGT normalizes the changes induced by IND treatment.

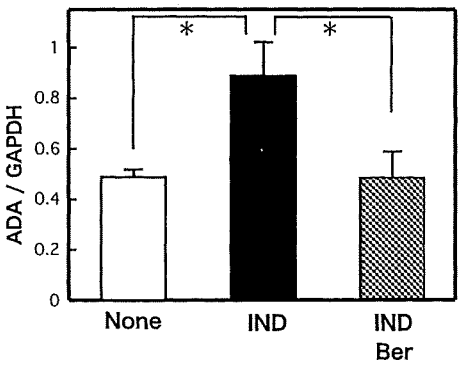

Fig. 6 Berberine reduced ADA mRNA expression in the small intestine. Small intestines were harvested at 24 h after the second injection of IND. Diet containing berberine at twice the concentration corresponding to that in 2% OGT was administered from the first IND injection until the end of experiment. $^*P < 0.05$, *t* test with Bonferroni correction. Data represent the means ± SEM ($n = 5$ per group)

Discussion

Several pathogenic factors of IND-induced enteropathy have been suggested [13, 14], which were PGs depletion after COX inhibition [15], increase of intestinal permeability after mitochondrial damage [16], exposure of luminal bacteria to mucosa [9], oxidative stress [17], nitric oxide [10], TNF-α [18], neutrophil infiltration [19] and microcirculatory changes [20–22].

In the present study, we demonstrated that the adenosine system, including ADA, plays an important role in IND-induced enteropathy and its amelioration by OGT, which indicates that the adenosine system is another option of the mechanism and therapeutic target of IND-induced enteropathy. Adenosine is a ubiquitous endogenous purine nucleoside, which exerts its various biological actions in many organs via cell surface adenosine receptors (A1, A2a, A2b, A3) [23]. Normally the extracellular adenosine concentration is strictly controlled by a set of synthetic, transport and metabolic molecules. However, in response to cellular damage (e.g. inflammation or ischemia), adenosine concentration is quickly elevated, which plays a prominent role in modulating inflammation and helps to maintain tissue integrity [24]. The cytoprotective functions

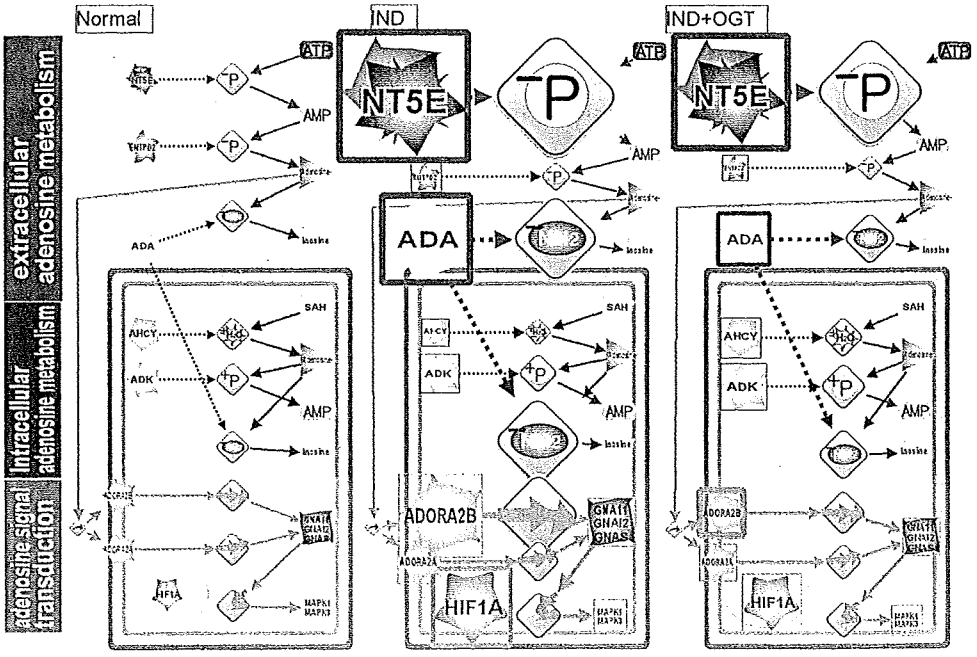

Fig. 7 Schematic representation of changes in gene expression of the adenosine system using Cell Illustrator Online (CIO). *NT5E* CD73/ectonucleotidase, *ADA* adenosine deaminase, *ADORA* adenosine receptor, *HIF1A* hypoxia inducible factor 1A, *GNA* G protein, *ADK* adenosine kinase

of adenosine have been suggested in several experimental colitis models by modulation of adenosine signaling. Indeed, adenosine has been proposed to form the basis of a novel therapeutic option for inflammatory bowel diseases (IBDs) [25, 26]. Furthermore, the prominent role of A2a receptors suggested by the present results is in good accordance with previous reports on both acute and chronic colitis models [27, 28].

Here, we showed that OGT decreased ADA mRNA expression which was increased by injection of IND. ADA is an enzyme that is largely responsible for the degradation of adenosine. The cellular concentration of adenosine is determined by the net balance of adenosine synthesis, transport and catabolism. Therefore, it is possible that OGT may increase the adenosine concentration by decreasing the amount of ADA. Inhibition of ADA as a possible therapeutic option for enteropathy was also suggested in a report by Antonioli et al. [29] where it was shown that an ADA inhibitor attenuates DNBS colitis. Survey and analysis of the results of microarray data (Fig. 7; Table 3) suggested that the genes involved in extracellular adenosine metabolism are most profoundly affected, which support the hypothesis that the effect of IND/OGT is closely related to the extracellular concentration of adenosine. Furthermore, because OGT decreased ADA mRNA in normal mice, the decrease of ADA may not be the result of a reduction in inflammation but an independent action executed by OGT.

Pouliot et al. [30] showed that adenosine upregulated COX-2 enzyme in human granulocytes, and suggested that adenosine might promote a self-limiting regulatory process through the increase of PGE2 generation. In our previous study, we showed that OGT elicited an increase in the number of COX-2 expressing cells in the lamina propria and in the production of mucosal PGE2. These observations could be explained in terms of an increase in the concentration of adenosine due to inhibition of ADA activity. However, because we did not determine the adenosine concentration, further extensive studies are necessary to clarify this point.

Investigation of active components using major isoquinoline alkaloids of OGT has revealed that two berberine-like alkaloids, berberine and coptisine, display preventive activity on IND-induced death. We focused the attention of the effects of berberine, because the alkaloid is readily available and ethically used in Japan. Berberine reduced the lethality by IND and decreased ADA mRNA expression in the small intestine (Figs. 5b, 6). However, treatment with berberine alone did not have sufficient efficacy on the lethality even if the dose was increased (Fig. 5b). Thus, we believe that additional ingredients may be responsible for the potent preventive effect of OGT against enteropathy.

In conclusion, guided by a transcriptome approach using MGP analysis, we have demonstrated the importance of the adenosine system in IND-induced enteropathy and its amelioration by OGT/berberine. This study addresses the possible efficacy of OGT as a treatment option for the adverse effect of NSAIDs on the small intestine. We believe that modulation of the adenosine system may provide an effective therapeutic strategy for NSAID-induced enteropathy.

References

1. Goldstein JL, Eisen GM, Lewis B, Gralnek IM, Zlotnick S, Fort JG. Video capsule endoscopy to prospectively assess small bowel injury with celecoxib, naproxen plus omeprazole, and placebo. Clin Gastroenterol Hepatol. 2005;3:133–41.
2. Maiden L, Thjodleifsson B, Theodors A, Gonzalez J, Bjarnason I. A quantitative analysis of NSAID-induced small bowel pathology by capsule enteroscopy. Gastroenterology. 2005;128:1172–8.
3. Graham DY, Opekun AR, Willingham FF, Qureshi WA. Visible small-intestinal mucosal injury in chronic NSAID users. Clin Gastroenterol Hepatol. 2005;3:55–9.
4. Bjarnason I, Hayllar J, MacPherson AJ, Russell AS. Side effects of nonsteroidal anti-inflammatory drugs on the small and large intestine in humans. Gastroenterology. 1993;104:1832–47.
5. Bjarnason I, Smethurst P, Fenn CG, Lee CE, Menzies IS, Levi AJ. Misoprostol reduces indomethacin-induced changes in human small intestinal permeability. Dig Dis Sci. 1989;34:407–11.
6. Niwa Y, Nakamura M, Ohmiya N, Maeda O, Ando T, Itoh A, et al. Efficacy of rebamipide for diclofenac-induced small-intestinal mucosal injuries in healthy subjects: a prospective, randomized, double-blinded, placebo-controlled, cross-over study. J Gastroenterol. 2008;43:270–6.
7. Maiden L, Thjodleifsson B, Seigal A, Bjarnason II, Scott D, Birgisson S, et al. Long-term effects of nonsteroidal anti-inflammatory drugs and cyclooxygenase-2 selective agents on the small bowel: a cross-sectional capsule enteroscopy study. Clin Gastroenterol Hepatol. 2007;5:1040–5.
8. Miura N, Fukutake M, Yamamoto M, Ohtake N, Iizuka S, Imamura S, et al. An herbal medicine orengedokuto prevents indomethacin-induced enteropathy. Biol Pharm Bull. 2007;30:495–501.
9. Robert A, Asano T. Resistance of germfree rats to indomethacin-induced intestinal lesions. Prostaglandins. 1977;14:333–41.
10. Whittle BJ, Laszlo F, Evans SM, Moncada S. Induction of nitric oxide synthase and microvascular injury in the rat jejunum provoked by indomethacin. Br J Pharmacol. 1995;116:2286–90.
11. Yamaguchi R, Yamamoto M, Imoto S, Nagasaki M, Yoshida R, Tsuiji K, et al. Identification of activated transcription factors from microarray gene expression data of Kampo medicine-treated mice. Genome Inform. 2007;18:119–29.
12. Nagasaki M, Doi A, Matsuno H, Miyano S. Genomic Object Net: I. A platform for modelling and simulating biopathways. Appl Bioinformatics. 2003;2:181–4.
13. Davies NM, Wallace JL. Nonsteroidal anti-inflammatory drug-induced gastrointestinal toxicity: new insights into an old problem. J Gastroenterol. 1997;32:127–33.
14. Konaka A, Kato S, Tanaka A, Kunikata T, Korolkiewicz R, Takeuchi K. Roles of enterobacteria, nitric oxide and neutrophil in pathogenesis of indomethacin-induced small intestinal lesions in rats. Pharmacol Res. 1999;40:517–24.

15. Vane JR. Inhibition of prostaglandin synthesis as a mechanism of action for aspirin-like drugs. Nat New Biol. 1971;231:232–5.
16. Somasundaram S, Rafi S, Hayllar J, Sigthorsson G, Jacob M, Price AB, et al. Mitochondrial damage: a possible mechanism of the "topical" phase of NSAID induced injury to the rat intestine. Gut. 1997;41:344–53.
17. Basivireddy J, Vasudevan A, Jacob M, Balasubramanian KA. Indomethacin-induced mitochondrial dysfunction and oxidative stress in villus enterocytes. Biochem Pharmacol. 2002;64:339–49.
18. Bertrand V, Guimbaud R, Tulliez M, Mauprivez C, Sogni P, Couturier D, et al. Increase in tumor necrosis factor-alpha production linked to the toxicity of indomethacin for the rat small intestine. Br J Pharmacol. 1998;124:1385–94.
19. Antoon JS, Perry MA. Role of neutrophils and mast cells in acute indomethacin-induced small bowel injury in the rat. J Gastroenterol. 1997;32:747–57.
20. Miura S, Suematsu M, Tanaka S, Nagata H, Houzawa S, Suzuki M, et al. Microcirculatory disturbance in indomethacin-induced intestinal ulcer. Am J Physiol. 1991;261:G213–9.
21. Nishizawa T, Suzuki H, Masaoka T, Iwasaki E, Hibi T. Reduced conscious blood flow in the stomach during non-steroidal anti-inflammatory drugs administration assessed by flash echo imaging. Scand J Gastroenterol. 2007;42:1040–4.
22. Nishizawa T, Suzuki H, Masaoka T, Hibi T. Education and imaging. Gastrointestinal: enhanced gastric mucosal blood flow in aspirin intoxication. J Gastroenterol Hepatol. 2007;22:2037.
23. Fredholm BB, IJzerman AP, Jacobson KA, Klotz KN, Linden J. International Union of Pharmacology. XXV. Nomenclature and classification of adenosine receptors. Pharmacol Rev. 2001;53:527–52.
24. Hasko G, Cronstein BN. Adenosine: an endogenous regulator of innate immunity. Trends Immunol. 2004;25:33–9.
25. Antonioli L, Fornai M, Colucci R, Ghisu N, Tuccori M, Del Tacca M, et al. Pharmacological modulation of adenosine system: novel options for treatment of inflammatory bowel diseases. Inflamm Bowel Dis. 2008;14:566–74.
26. Kolachala VL, Bajaj R, Chalasani M, Sitaraman SV. Purinergic receptors in gastrointestinal inflammation. Am J Physiol Gastrointest Liver Physiol. 2008;294:G401–10.
27. Odashima M, Bamias G, Rivera-Nieves J, Linden J, Nast CC, Moskaluk CA, et al. Activation of A2A adenosine receptor attenuates intestinal inflammation in animal models of inflammatory bowel disease. Gastroenterology. 2005;129:26–33.
28. Cavalcante IC, Castro MV, Barreto AR, Sullivan GW, Vale M, Almeida PR, et al. Effect of novel A2A adenosine receptor agonist ATL 313 on *Clostridium difficile* toxin A-induced murine ileal enteritis. Infect Immun. 2006;74:2606–12.
29. Antonioli L, Fornai M, Colucci R, Ghisu N, Da Settimo F, Natale G, et al. Inhibition of adenosine deaminase attenuates inflammation in experimental colitis. J Pharmacol Exp Ther. 2007;322:435–42.
30. Pouliot M, Fiset ME, Masse M, Naccache PH, Borgeat P. Adenosine up-regulates cyclooxygenase-2 in human granulocytes: impact on the balance of eicosanoid generation. J Immunol. 2002;169:5279–86.

Tumor necrosis factor-α mediates hyperglycemia-augmented gut barrier dysfunction in endotoxemia*

Satoshi Yajima, MD; Hiroshi Morisaki, MD; Ryohei Serita, MD; Takeshi Suzuki, MD; Nobuyuki Katori, MD; Takashi Asahara, PhD; Koji Nomoto, PhD; Fujio Kobayashi, BA; Akitoshi Ishizaka, MD; Junzo Takeda, MD

Objective: To examine whether hyperglycemia would augment gut barrier dysfunction and inflammatory responses in endotoxemic rats, and simultaneously to clarify the roles of tumor necrosis factor (TNF)-α in alterations of gut mucosal permeability associated with hyperglycemia.

Design: Prospective randomized animal study.

Setting: University research laboratory.

Subjects: Male Wistar rats treated with lipopolysaccharide (LPS) injection.

Interventions: After LPS injection (4 mg/kg), rats were randomly allocated into group S (n = 6), group G (n = 7), or group GI (n = 8) with continuous infusion of different fluid solutions: normal saline, 40% glucose or 10% glucose mixed with insulin, respectively. Blood glucose, insulin, and proinflammatory cytokines, accompanied by gut mucosal permeability using an *in situ* loop preparation of gut with fluorescence isothiocyanate-conjugated dextran, were measured. Bacterial growth or alterations in mesenteric lymph nodes and cecal contents were also assessed. We further determined the roles of TNF-α using an inhibitor of TNF-α converting enzyme in gut barrier dysfunction under the same experimental settings.

Measurements and Main Results: Hyperglycemia over 400 mg/dL was achieved and kept in group G during the study period whereas normoglycemia was preserved in group S and GI, the latter of which showed the similar extent of hyperinsulinemia to group G. Plasma concentrations of fluorescence-labeled dextran and TNF-α in group G were significantly higher vs. group S and GI, and the number of bacteria found in mesenteric lymph nodes in group G was greater compared with group S. Intestinal environments including microflora and organic acids were not altered by blood glucose or insulin level. Inhibiting conversion of membrane-bound to soluble type of TNF-α restored gut mucosal permeability augmented by hyperglycemia.

Conclusions: These findings indicate that hyperglycemia deteriorates LPS-elicited gut barrier dysfunction and bacterial translocation independently of plasma insulin level, and that TNF-α mediates such mucosal dysfunction of gut in endotoxemia. (Crit Care Med 2009; 37:1024–1030)

Key Words: hyperglycemia; insulin; endotoxin; TNF-α converting enzyme; gut mucosal permeability

Hyperglycemia has been recognized as a consequential risk factor to increase the mortality and morbidity in critically ill even without diabetes mellitus (1, 2). Clinical trials demonstrated that intensive insulin therapy to regulate blood glucose level <110 mg/dL improved the outcome of both medical and surgical patients who were admitted in intensive care units (3, 4), whereas the most recent study alarmed that such tight control of blood glucose increased a potential threat for serious adverse events associated with hypoglycemia (5). Previous reports showed that acute hyperglycemia enhanced systemic inflammatory responses including oxidative stress and cytokine production (6), which were lessened by hyperinsulinemic euglycemia in animal models of endotoxemia (7). Although a multivariate analysis of the clinical data suggests that normoglycemia is the key factor rather than insulin infusion to improve the outcome (8), insulin by itself attenuated endotoxin-induced increases of nitric oxide (NO) and superoxide production, and subsequently slowed the progression of lung injury (9). Nevertheless, it still remains unclear which factor, keeping normoglycemia or plasma insulin level, is the determinant to improve the outcome in critically ill.

Despite being long considered as a nonvital organ, gut has now become one of therapeutic targets in critically ill (10). A loss of barrier function, regulated by several factors such as NO and tumor necrosis factor (TNF)-α (11, 12), permits an invasion of intraluminal bacteria and/or toxins into systemic bloodstream and lymph nodes, subsequently augments systemic inflammatory responses and the development of multiple organ failure (10). Because hyperglycemia modulates inflammatory responses involving both NO and TNF-α (13), we hypothesized that hyperglycemia damaged gut mucosa and evoked bacterial translocation, resulting in the increase of modality-like positive blood culture as shown in clinical trials (3, 4). In addition, excessive abnormality of bacterial flora in gut is another element to induce bacterial translocation and to determine the outcome in critically ill (14). In an endotoxemic rat model, we, therefore, evaluated the effects of hyperglycemia and plasma insulin level on gut barrier function, intestinal flora, and production of proinflammatory cytokines. As a second aim of this study, we further examined the roles of TNF-α in the relationship between hyperglycemia and gut barrier dysfunction in endotoxemia.

*See also p. 1160.

From the Departments of Anesthesiology (SY, RS, TS, NK, HM, JT), and Medicine (AI), Keio University School of Medicine, Tokyo, Japan; Yakult Central Institute for Microbiological Research (TA, KN), Tokyo, Japan; Research & Development Division (FK), Tanabe-Mitsubishi Pharma Corporation, Yokohama, Japan.

Supported by funds from Keio Medical Research Funds and Yakult Bioscience Foundation.

The authors have not disclosed any potential conflicts of interest.

For information regarding this article, E-mail: morisaki@z8.keio.jp

DOI: 10.1097/CCM.0b013e31819b53b6

METHODS

This study protocol was approved by the animal care and use committee of Keio University School of Medicine in accordance with the National Institute of Health.

Animal Model. Male Wistar rats, weighing 220–250 g, were studied after a 3–7 days period of acclimatization in our laboratory. With isoflurane anesthesia in oxygen, the jugular vein and carotid artery were cannulated with a catheter (PE50; Intermedic, Sparks, MD) under sterile condition. After this preparation, the animals were placed in a metabolic cage that allowed time for awakening and stabilization for 1 hour. Arterial catheter was connected to a pressure transducer (Nihon Kohden, Tokyo, Japan) to record the mean arterial pressure and heart rate on a polygraph recorder (Power lab, AD Instruments, Mountain View, CA). Then, all animals received intravenous injection of 4 mg/kg lipopolysaccharide (LPS) (*Escherichia coli*, Sigma Chemicals, St. Louis, MO) and fluid therapy for the next 3 hours.

Study Protocol 1. After the preparatory surgery described above, 21 animals were randomized into three groups using a computer-generated random number: group S (n = 6) received intravenous infusion of normal saline, group G (n = 7) received 40% glucose solution (Ohtsuka Pharma, Tokushima, Japan), and group GI (n = 8) received 10% glucose solution (Ohtsuka Pharma) mixed with insulin (8 $mU \cdot kg^{-1} \cdot min^{-1}$) (Insulin Human, Novolin-R injection, Novo-Nordisk, Copenhagen, Denmark). All solutions were infused at the rate of 10 $mL \cdot kg^{-1} \cdot hr^{-1}$. The target glucose level in group G was 300–350 mg/dL commonly applied in previous experimental studies (15, 16) whereas those in group S and GI were ranged at 80–110 mg/dL as described by van den Berghe et al (3, 4). Our pilot study showed a continuous infusion of glucose and insulin mixture reached approximately within each blood glucose range, accompanied by hyperinsulinemia in rats. Arterial blood was sampled for measuring blood glucose levels (ACCU-chek; Roche Diagnostics, Basel, Switzerland) at baseline, 1, 2, and 3 hour after the randomization. Simultaneously, at 3-hour study period, plasma concentration of insulin, cytokines, and nitric oxide metabolites (NOx) were measured. Thereafter, laparotomy was performed under isoflurane anesthesia and sterile condition for the examination of gut mucosal permeability. In a separate series of experiments, sampling of mesenteric lymph nodes (MLNs) and cecal contents for the assessment of intestinal flora from 21 animals (group S: n = 6, group G: n = 7, and group GI: n = 8) was performed as described below. To evaluate intestinal microbes and plasma insulin level in normal rats, we analyzed the samples obtained from four sham rats which received the same catheterization and fluid therapy with saline without LPS injection.

Study Protocol 2. Following the catheterization, another 32 rats which received the same amount of LPS were randomized into four groups: group S (n = 8) received normal saline, group ST (n = 9) received normal saline containing 0.3 mg/mL of tumor necrosis factor converting enzyme (TACE) inhibitor (Y-41654; Tanabe-Mitsubishi Pharma, Ohsaka, Japan), group G (n = 8) received 40% glucose solution, and group GT (n = 7) received 40% glucose solution containing 0.3 mg/mL of Y-41654. All solutions were infused at the rate of 10 $mL \cdot kg^{-1} \cdot hr^{-1}$. At the 3-hour study period, arterial blood was obtained for measurements of several markers described in Study Protocol 1 section, and thereafter laparotomy was performed for examination of gut mucosal permeability as described below. Y-41654, a water-soluble compound with a molecular weight of approximately 700 and a half-life of 30 minutes in rat blood, has a peptide-mimicking hydroxamate structure which facilitates chelation of the zinc ion in the active site of the TACE. This compound was found to show high potency against TACE in substrate assays (data not shown), suggesting that it behaves as a competitive inhibitor.

Measurements of Gut Mucosal Permeability. We determined gut mucosal permeability by using fluorescein isothiocyanate-conjugated dextran (FD4) with a molecular weight of 4000 Da, as described previously (17). Briefly, the abdomen was opened for preparation of an *in situ* loop of gut. After removal of undigested food in observed segment of ileum with phosphate-buffered saline (pH 7.4), double ligatures at both ends were made on the 10-cm length of terminal ileum. Through a cannula placed into this segment of terminal ileum, FD4 (10 mg in 1 mL of phosphate-buffered saline, Sigma, St. Louis, MO) was injected, which resulted in a slight distension of intestinal loop. After 30 minutes, blood samples from both portal vein and artery were obtained and centrifuged, and plasma FD4 concentrations were measured at an excitation wavelength of 480 nm and an emission wavelength of 520 nm using fluorescence spectrometry (Spectrofluorophotometer: RF-1500, Shimadzu, Kyoto, Japan). Results were corrected for plasma protein contents measured by Lowry method.

Sampling of MLNs and Cecal Contents. To perform the sampling of MLNs and cecal contents under sterile condition, another 21 rats, which were randomized and treated with fluid therapy for 3 hours according to Study Protocol 1, were examined. After laparotomy, cecum and distal ileum were externalized, and three MLNs in each rat were randomly sampled and homogenized in 0.5 mL sterilized phosphate buffer solution. The MLNs in phosphate buffer solution were submerged in RNAlater (Ambion, Austin, TX), followed by being stored under conditions where RNA degradation would normally take place rapidly. Blood (1 mL) obtained from portal vein was mixed with sodium citrate (0.38%, wt/vol) and RNAprotect™ bacterial reagent (Qiagen, Hilden, Germany). Thereafter, a 10-cm segment of distal ileum was dissected and its contents were collected into the tube including 2 mL RNAlater and mixed vigorously for the examination of gut flora in MLNs as described below. The contents of cecum were collected for examination of organic acid concentrations and pH as described below. All samples were weighed and stored at −20°C until further examinations.

Determination of RNA, Bacteria, and Organic Acid Concentrations in Gut or MLNs. After serial 1/10 dilutions of all samples were made in RNAlater, they were added to two volumes of RNAprotect™ bacterial reagent, and then the preparations were incubated for 5 minutes at room temperature. After centrifugation of each mixture at 5000 g for 10 minutes, the supernatant was discarded and the pellet was stored at −80°C until it was used for extraction of RNA. RNA was isolated using the method described elsewhere (18). Finally, the nucleic acid fraction was suspended in 50 μL-nuclease-free water. A standard curve was generated with reverse transcription-quantitative polymerase chain reaction data (using the threshold cycle [C_T] value, the cycle number when the threshold fluorescence was reached) and the corresponding cell count, which was determined microscopically with 4,6-diamidino-2-phe-nylindole (Vector Laboratories, Burlingame, CA) staining (19) for dilution series of the standard strains described elsewhere (20). For determination of the bacteria presented in samples, three serial dilutions of an extracted RNA sample were used for reverse transcription-quantitative polymerase chain reaction, and the C_T values in the linear range of the assay were applied to the standard curve generated in the same experiment to obtain the corresponding bacterial cell count in each nucleic acid sample and then converted to the number of bacterial per sample. The specificity of the reverse transcription-quantitative polymerase chain reaction assay using the group- or species-specific primers was determined as described previously (20).

The contents of cecum were homogenized in 1 mL distilled water, and centrifuged at 10,000 rpm at 4°C for 10 minutes. A mixture of 0.9 mL of the resulting supernatant and 0.1 mL of 1.5 mol/L perchloric acid was mixed in a glass tube, and allowed to stand at 4°C for 12 hours. The suspension was then passed through a filter with a pore size of 0.45 μm (Millipore Japan, Tokyo). The sample was analyzed for organic acids by high-performance liquid chromatography, and the concentrations of organic acids were calculated with the use of external standards, and the reproducibility and stability of these measurements were described previously (21).

Immunohistochemical Staining of Ileal Mucosa for Inducible Nitric Oxide Synthase (iNOS). In a separate series of experiments, the iNOS expression on ileum was determined by immunohistochemistry. At 3-hour study period, three rats in each study group with three sham rats were anesthetized, and terminal ileum was excised, immediately frozen in OCT compound (Tissue-Tek; Sakura Finetek Japan, Tokyo, Japan), and then sectioned into 8-μm square. Tissue sections were fixed with 10% neutral buffered formalin for 10 minutes, and washed with Tris buffer solution. They

were treated with Protein Block (Dako, Glostrup, Denmark) for 10 minutes, and incubated with 2 μg/mL anti-mouse iNOS rabbit polyclonal antibody (Wako Pure Chemical Industry, Osaka, Japan) at 4°C overnight, and washed with Tris buffer solution. Endogenous peroxidase activity was blocked with 0.3% hydrogen peroxide in methanol for 30 minutes. They were treated with Biotin blocking system (Dako) and incubated with biotin-conjugated goat anti-rabbit immunogloburin (Dako) diluted 1:600, for 30 minutes at reverse transcription. After washing with Tris buffer solution, they were treated with peroxidase-conjugated streptavidin (Nichirei Biosience, Tokyo, Japan) for 5 minutes. Peroxidase activity was visualized by diaminobenzidine. The sections were counterstained with Mayer's Hematoxylin (Mutoh Chemical, Tokyo, Japan), dehydrated, and then mounted with Malinol (Mutoh). Ten images per each sample were randomly photographed using a microscope attached modular photomicrographic system (Nikon Eclipse TS 100, Nikon, Tokyo). The immunostaining area of the ileum was measured using computer software (NIH image 1.63 software, National Institutes of Health, Bethesda, MD) in a blinded manner (22), and the ratio of this area to all field of the image was determined as the expression density of iNOS.

Biochemical Analyses. Arterial blood at 3-hour study period was centrifuged at 2500 rpm for 10 minutes at 4°C, and then stored at −80°C for measurements of insulin, cytokines, and NOx. Plasma insulin concentration was measured in duplicate with a specific enzyme-linked immunosorbent assay method using commercially available enzyme-linked immunosorbent assay kit (Mercodia AB, Uppsala. Sweden), which showed cross-reactivity with human insulin. TNF-α and interleukin (IL)-1β were measured in duplicate by enzyme-linked immunosorbent assay using commercially available kits (Immunoassay Kit, Biosource International, CA). Briefly, after incubation in immobilized antibody and a biotinylated antibody specific for each cytokine, streptavidine-peroxidase is added. This binds to the biotinylated antibody to complete the four-member sandwich. Then, a substrate solution is added, which is acted on by the bound enzyme to produce color. The intensity of this colored product is directly proportional to the concentration of each cytokine. NO release was assessed by the determination of plasma NO metabolites (nitrate and nitrite; NOx) by colorimetric assay using the enzyme nitrate reductase (Oxford Biomedical Research Oxford, MI). The intensity was measured using a plate analyzer (ETY-3A, Toyosokki, Tokyo, Japan).

Statistical Analyses. Data were expressed as mean ± SD unless otherwise specified. Data obtained at various periods were analyzed by two-way analysis of variance with repeated measures using a statistical software package of SPSS/15.0J for Windows (SPSS Inc, Chicago, IL). One-way analysis of variance was applied to examine the data obtained at one study period such as portal FD4, cytokines, and blood gas analyses. Kruskal-Wallis test was used to examine the nonparametric data such as intestinal microbes. *Post hoc* test was made by using Tukey's test. Values of $p < 0.05$ were considered statistically significant.

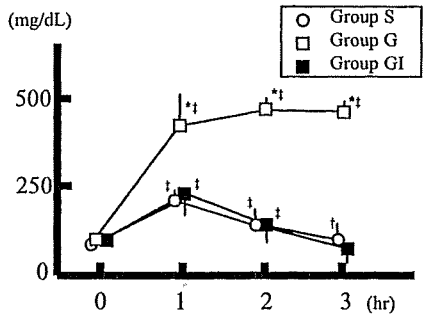

Figure 1. Changes of blood glucose concentrations during the 3-hour study period in endotoxemic rats treated with saline, glucose, and glucose mixed with insulin solutions. Values are expressed as means ± SD. Group S (n = 6) = saline alone, group G (n = 7) = 40% glucose solution, and group GI (n = 8) = 10% glucose mixed with insulin solution. Significance *$p < 0.01$ vs. group S and GI, †$p < 0.05$, ‡$p < 0.01$ vs. 0 hour.

RESULTS

All animals in both Study protocol 1 and 2 survived for 3-hour study periods.

Table 1. Arterial blood gas and lactate levels in endotoxemic rats after 3 hr-infusion of saline, glucose, and glucose mixed with insulin solutions

	Group S (n = 6)	Group G (n = 7)	Group GI (n = 8)
pH	7.43 ± 0.06	7.35 ± 0.04[a]	7.45 ± 0.07[c]
PaO_2 (mm Hg)	99 ± 9	100 ± 12	98 ± 20
$PaCO_2$ (mm Hg)	27.3 ± 3.4	26.0 ± 4.8	27.3 ± 6.4
Base excess	−6.3 ± 1.4	−9.9 ± 2.5	−5.8 ± 3.1[c]
Lactate (mmol/L)	1.6 ± 0.3	4.7 ± 0.6[b]	2.4 ± 0.5[a,d]
Osmolarity (mOsm/L)	287 ± 2	293 ± 5	289 ± 5

Data were expressed as mean ± SD.
Group S, saline alone; Group G, 40% glucose solution; Group GI, 10% glucose solution mixed with insulin.
Significance: [a]$p < 0.05$, [b]$p < 0.01$ vs. Group S, [c]$p < 0.05$, [d]$p < 0.01$ vs. Group G.

Study Protocol 1

Changes of Systemic Hemodynamics, Blood Glucose, and Insulin Concentrations. At the baseline (0 hour), the values of mean arterial pressure, heart rate, and blood glucose concentration were not different between the groups. Overall changes of mean arterial pressure and heart rate were trivial throughout the study periods (data not shown), suggesting that the outcome of the present study was unlikely to be dependent on systemic hemodynamics. Blood glucose level in group G was significantly increased at 1 hour and remained higher than the level of 400 mg/dL, which was to some extent higher than we planned (Fig. 1). Those in group S and GI were slightly but significantly elevated at 1 and 2 hour vs. the baseline (0 hour), and became down to the baseline level, i.e., approximately at 100 mg/dL. On the other hand, plasma insulin concentration at 3-hour study period remained low level in group S, but group G and GI showed a marked increase (6.2 ± 4.7 μg/L vs. 124.1 ± 13.4 μg/L and 112.7 ± 1.0 μg/L, respectively; $p < 0.001$). Because of necessary blood sampling limitation, we did not assess the changes of plasma insulin levels during the 3-hour study period. In all sham rats, plasma insulin level was undetectable, i.e., less than 3 μg/L. Collectively, under similar extent of hyperinsulinemia developed, the animals in group G and GI showed stable hyperglycemia and normoglycemia, respectively, for 3-hour study period.

Arterial blood gas analyses at 3 hours after LPS injection showed that arterial pH in all groups were slight metabolic acidosis but were basically compensated well by respiratory alkalosis (Table 1). However, arterial lactate level in group G showed a significant elevation compared with group S and GI. Serum osmolarity, calculated by the standard formula including the values of plasma sodium ion, glucose and urea nitrogen levels, stayed within normal ranges at 3-hour study period in all study groups.

Gut Mucosal Permeability, Cytokines, and NO. Plasma FD4 concentration showed a marked increase in group G compared with the other two groups (Fig. 2). Because portal FD4 concentration in group S was slightly higher than normal value, usually being less than 0.15-mg/mg protein in rats, hyperglycemia augmented gut mucosal permeability which was already elevated by endotoxin injection. Arterial concentration of FD4 showed the similar results as portal levels (data not shown). Simultaneously, arterial concen-

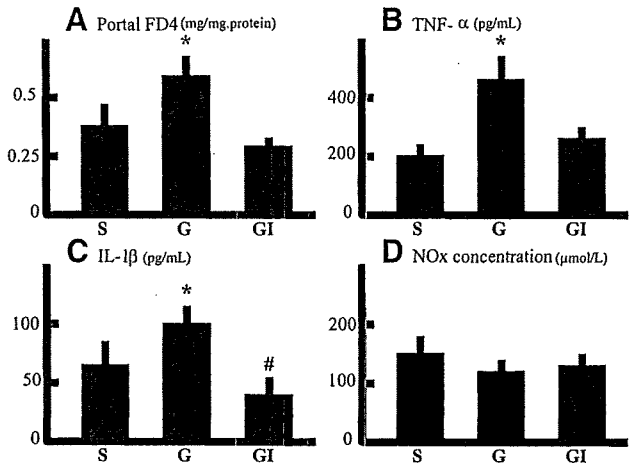

Figure 2. Plasma concentrations of fluorescence-conjugated dextran (*FD4*), tumor necrosis factor-α (*TNF-α*), interleukin-1β (*IL-1β*), and nitric oxide metabolites (*NOx*) at 3-hour study period in endotoxemic rats treated with saline, glucose, and glucose mixed with insulin solutions. Values are expressed as means ± SD. Group S (n = 6) = saline alone, group G (n = 7) = 40% glucose solution, group GI (n = 8) = 10% glucose mixed with insulin solution. Significance: *$p < 0.05$ vs. group S and GI, #$p < 0.05$ vs. group S.

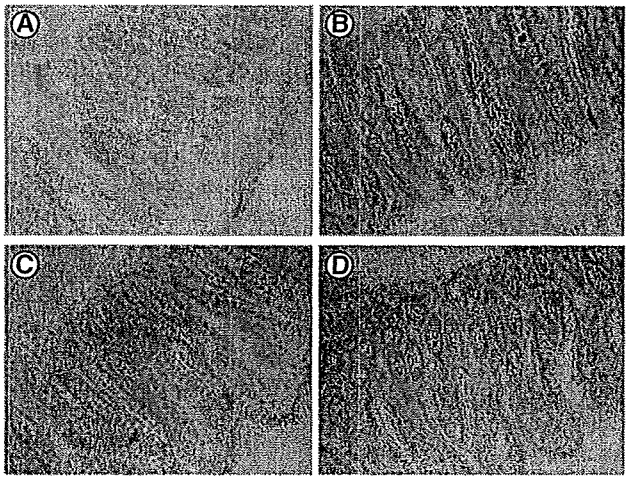

Figure 3. Representative micrographs of immunohistochemical staining of ileal mucosa for inducible nitric oxide synthase (iNOS) in sham and endotoxemic rats treated with saline, glucose, and glucose mixed with insulin solutions. Positive staining for iNOS is brown. *A*, A representative immunostaining of ileal mucosa from a Sham rat. *B–D*, A representative immunostaining of ileal mucosa from a rat in group S, G, and GI, respectively. Note that the density of iNOS expression is apparently augmented vs. the Sham rat but appears to be similar between the LPS-treated groups.

trations of proinflammatory cytokines, TNF-α, and IL-1β, were significantly elevated in group G vs. group S and GI. On the other hand, plasma concentrations of NOx, considered as a marker of NO production, were similar between the three groups. Weak but constant staining of iNOS was observed in microvilli of mucosal layer in sham-operated rats (Fig. 3*A*). Compared with the sham, LPS infusion in all study groups increased iNOS expression on the surface of villus epithelial cells and in crypts more intensely as shown in Figure 3, *B–D*. However, no significant differences of iNOS expression were not found between the three LPS-treated groups (data not shown), indicating that LPS injection was a dominant factor to iNOS on ileal mucosa independently of blood glucose or insulin level.

Bacterial Microflora and Organic Acids in Gut and Bacteria in MLNs. In sham rats, the majority of intestinal flora consisted of *Clostridium group* and *Bacteroides fragilis* in *Obligate anaerobes*, and *Lactobacillus* and *Enterococcus* in *Facultative microbe* whereas pathogenic microbes such as *Staphylococcus* or *Pseudomonas* remained relatively low level (Table 2). The three study groups showed the similar tendency to the sham, suggesting that LPS injection did not cause significant alterations of intestinal flora for 3-hour periods. Total organic acids dominated by acetic, propionic, and butyric acids in all LPS-treated groups appeared to be depressed vs. the sham group (Table 3). No significant differences were found between the study groups. Simultaneously, pH level in cecal contents was kept higher vs. the sham, but no statistical difference was found between the three study groups.

Total counts of bacteria present in MLNs of group G were significantly higher vs. group S, whereas the former appeared to be higher vs. group GI but it did not reach statistical significance (Fig. 4). No bacteria was found in the MLNs of all animals in group S, whereas the numbers of animals which showed no bacteria in MLNs were 1 in group G and 3 in group GI, respectively.

Study Protocol 2

Roles of TNF-α in Hyperglycemia-Related Gut Barrier Function and Cytokines. The infusion of Y-41654 did not modulate blood glucose levels at 3 hours in both normoglycemia and hyperglycemia (data not shown). Blood gas analyses at 3-hour period were not altered significantly with Y-41654 infusion whereas hyperglycemia group showed mild metabolic acidosis with a slight but significant elevation of arterial lactate (Table 4).

Plasma FD4 concentration, a marker of gut mucosal permeability, was not altered by treatment with a TACE inhibitor in normoglycemia whereas hyperglycemia-augmented mucosal permeability was significantly reduced by inhibiting TACE activity (Fig. 5*A*). Figure 5*B* shows that TACE inhibitor treatment significantly depressed the production of TNF-α, which was excessively discharged by endotoxin injection, in normoglycemia, and simultaneously did reduce the excessive discharges of TNF-α in hyperglycemia. Figure 5*C* shows that TACE inhibitor treatment did not significantly modulate IL-1β discharges in either normoglycemia or hyperglycemia group. NOx levels were not different between these four study groups (Fig. 5*D*).

DISCUSSION

The present study demonstrates that hyperglycemia augments endotoxin-induced gut barrier dysfunction, subsequently inducing bacterial translocation into MLNs, and concurrently excessive production of proinflammatory cytokines such as TNF-α and IL-1β. The regulation of blood glucose level with insulin infusion ameliorates such dysfunction of gut mucosal barrier in en-

Table 2. Intestinal flora in sham or endotoxemic rats after 3 hr-infusion of saline, glucose, and glucose mixed with insulin solutions

	Group S (n = 6)	Group G (n = 7)	Group GI (n = 8)	Sham (n = 4)
Obligate anaerobes				
Clostridium leptum subgroup	9.1 ± 0.6	8.7 ± 1.3	9.6 ± 0.2	9.7 ± 0.4
Clostridium coccoides group	9.9 ± 0.7	9.6 ± 1.3	10.3 ± 0.3	10.3 ± 0.4
Bacteroides fragilis group	9.3 ± 0.8	8.7 ± 1.4	9.8 ± 0.4	9.8 ± 0.3
Bifidobacterum	7.9 ± 0.8	7.9 ± 1.4	8.3 ± 0.6	8.8 ± 0.4
Atopobium cluster	8.1 ± 0.5	7.8 ± 1.2	8.4 ± 0.2	8.2 ± 0.2
Prevotella	9.0 ± 0.7	8.4 ± 1.2	9.5 ± 0.2	9.4 ± 0.3
Facultative anaerobes and aerobes				
Lactobacillus	9.8 ± 0.6	9.6 ± 0.9	10.2 ± 0.3	10.1 ± 0.4
Enterobacteriaceae	7.1 ± 1.1	6.1 ± 1.0	7.1 ± 0.6	6.4 ± 0.7
Enterococcus	8.4 ± 0.8	8.1 ± 0.7	8.3 ± 0.3	8.4 ± 0.1
Staphylococcus	6.0 ± 0.9	5.7 ± 0.9	6.1 ± 0.8	6.1 ± 0.2
Pseudomonas	< 2.4	< 2.4	< 2.4	< 2.4
Total microbes	10.3 ± 0.6	10.2 ± 0.3	10.8 ± 0.1	10.8 ± 0.1

Data were expressed as mean ± SD (bacteria/g-intestinal contents).

Group S, saline alone; Group G, 40% glucose solution; Group GI, 10% glucose solution mixed with insulin; Sham, saline without endotoxin injection.

No significant differences of intestinal microflora were found between the groups.

Table 3. Organic acids and pH of cecal contents in endotoxemic rats after 3 hr-infusion of saline, glucose, and glucose mixed with insulin solutions

	Group S (n = 6)	Group G (n = 7)	Group GI (n = 8)	Sham (n = 4)
Total organic acid	57.8 ± 18.8	66.5 ± 19.8	65.9 ± 21.9	76.6 ± 23.1
Acetic acid	34.1 ± 7.6	37.6 ± 8.4	38.6 ± 10.9	47.7 ± 15.9
Propionic acid	11.8 ± 2.5	12.6 ± 4.7	12.1 ± 5.0	14.1 ± 5.1
Butyric acid	4.6 ± 2.4	5.7 ± 3.0	6.9 ± 2.8	11.2 ± 1.2
Succinic acid	1.5 ± 1.0	1.3 ± 0.7	1.1 ± 0.5	1.3 ± 0.4
Lactic acid	5.9 ± 4.5	7.7 ± 5.5	7.1 ± 5.1	2.4 ± 1.7
Formic acid	0	0	0.2 ± 0.4	0.1 ± 0.5
Isovaleric acid	2.4 ± 0.4	2.3 ± 0.3	2.4 ± 0.5	0
Valeric acid	1.6 ± 0.5	1.6 ± 0.3	1.1 ± 0.1	0
pH	7.37 ± 0.44	7.35 ± 0.53	7.41 ± 0.39	7.22 ± 0.29

Data were expressed as mean ± SD.

Organic acids (μmol/g-intestinal contents).

Group S, saline alone; Group G, 40% glucose solution; Group GI, 40% glucose solution mixed with insulin solution; Sham, saline without endotoxin injection.

There were no significant differences in all organic acids and pH between the study groups.

dotoxemia, accompanied by inhibition of excessive production of proinflammatory cytokines. Although previous study demonstrated that increased insulin administration is positively associated with poor outcome regardless of the prevailing blood glucose level (23), the present study showed that hyperglycemia rather than plasma insulin level played a significant role in the regulation of gut mucosal permeability, possibly associated with the modality and mortality in critically ill. Additionally, inhibiting the conversion of membrane-bound to soluble TNF-α plays a key role in the hyperglycemia-augmented gut barrier dysfunction evoked by endotoxin. Collectively, these findings indicate that control of blood glucose in critically ill is of great consequence in the preservation of gut barrier function through TNF-α discharge-dependent mechanisms.

In the present study, abnormal overgrowth and/or distribution of bacterial microflora in gut lumen were not found but pathogenic bacteria were translocated into the MLNs only in group G. Thus, hyperglycemia did not modulate microflora but facilitate the translocation of pathogenic microbes through increased mucosal permeability of gut. Because the transcription of rRNA and production of ribosome are extremely greater in viable vs. nonviable bacteria, the total amount of rRNA produced by nonviable bacteria could be ignored (24). Previous study clearly demonstrated that reverse transcription-quantitative polymerase chain reaction, highly correlated with conventional culture, was a valuable method to assess the number of viable microbes by targeting rRNA from bacteria (20). Another important finding of the present study was to show that total organic acids in cecal contents were apparently reduced in all LPS-treated groups vs. the Sham animals. As energy substrates, short-chain fatty acids such as butyric, propionic, and acetic acids produced by intestinal microflora contributed to the preservation of gut homeostasis and proliferation of epithelial injury (25, 26). On the other hand, intestinal pH, modulating intraluminal microflora, absorption ability, and activity of digestive enzymes (27), was not affected by blood glucose or insulin level, suggesting that intraluminal environments were not directly associated with hyperglycemia or hyperinsulinemia under endotoxemia. Given these findings, at least for 3-hour examination period, LPS injection, rather than the changes of blood glucose or insulin level, deteriorates the production pathway of organic acids by intestinal microflora, and subsequently modulates mucosal function. However, we need to be cautious that bacterial analysis of stool is a complicated procedure and the results might be depending on the intestinal segment as described previously (28).

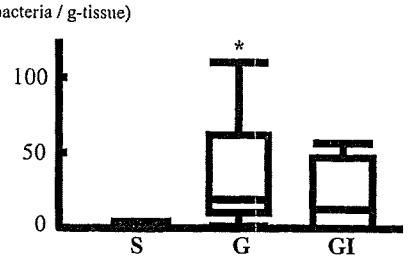

Figure 4. Total bacterial counts in mesenteric lymph nodes of endotoxemic rats treated with saline, glucose, and glucose mixed with insulin solutions. Group S (n = 6) = saline alone, group G (n = 7) = 40% glucose solution, group GI (n = 8) = 10% glucose mixed with insulin solution. The box represents the 25th to 75th percentiles in which black line is the median. The extended bars represent the 10th to 90th percentiles. Significance: *$p < 0.05$ vs. group S.

Several mechanisms to regulate gut barrier function have been proposed to date. Among them, endogenous production of NO plays the most important role in the modulation of gut permeability (11, 29) although NO is known to have paradoxic effects on gastrointestinal perfusion and integrity depending on its concentrations (30). In sepsis, up-regulation of iNOS expression leads to a prolonged increase of NOx in tissue and plasma levels (31). Indeed, expression of iNOS on mucosal layer was apparently augmented in all LPS-treated animals vs. the sham, whereas we were able to find neither significant alter-

Table 4. Arterial blood gas and lactate levels in endotoxemic rats after 3 hr-infusion of saline or glucose solution, with or without tumor necrosis factor converting enzyme (TACE) inhibitor

	Group S (n = 8)	Group ST (n = 9)	Group G (n = 8)	Group GT (n = 7)
pH	7.43 ± 0.03	7.45 ± 0.04	7.37 ± 0.05[a,b]	7.40 ± 0.07
PaO_2 (mmHg)	85 ± 7	87 ± 7	95 ± 7	88 ± 8
$PaCO_2$ (mmHg)	29 ± 2	28 ± 5	23 ± 5	25 ± 6
Base excess	−5 ± 2	−4 ± 2	−12 ± 3[a,b]	−10 ± 3[a,b]
Lactate (mmol/L)	1.3 ± 0.5	1.1 ± 0.2	5.1 ± 0.8[a,b]	4.2 ± 1.1[a,b]

Data were expressed as mean ± SD.

Group S, saline alone; Group ST, saline with TACE inhibitor; Group G, 40% glucose solution alone; Group GT, 40% glucose solution with TACE inhibitor.

Significance: [a]p <0.05 vs. Group S; [b]p <0.05 vs. Group ST.

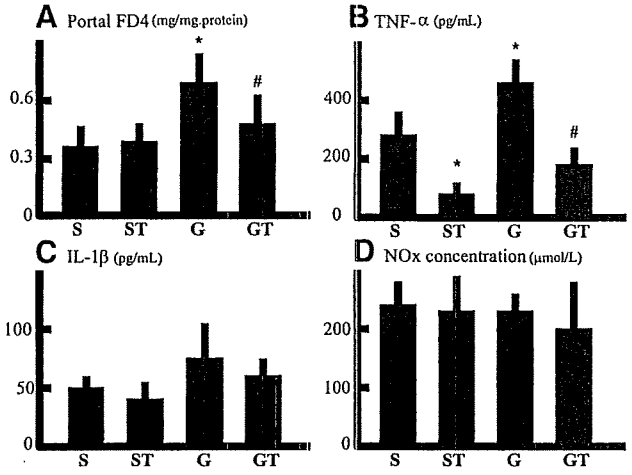

Figure 5. Plasma concentrations of fluorescence-conjugated dextran (*FD4*), tumor necrosis factor-α (*TNF-α*), interleukin-1β (*IL-1β*), and nitric oxide metabolites (*NOx*) in endotoxemic rats after 3–hour infusion of saline or glucose solution with or without tumor necrosis factor converting enzyme (TACE) inhibitor. Group S (n = 8) = saline alone, group ST (n = 9) = saline with TACE inhibitor, group G (n = 8) = 40% glucose solution alone, group GT (n = 7) = 40% glucose solution with TACE inhibitor. Values are expressed as means ± SD. Significance: *p < 0.05 vs. group S, #p < 0.05 vs. group G.

ations of plasma NOx levels nor intensity of iNOS expression using immunohistochemical study in this hyperglycemia model. Consequently, the local production of iNOS protein on the mucosal layer and plasma NO production is unlikely to regulate hyperglycemia-augmented gut barrier dysfunction evoked by endotoxin. However, recent study showed that circulating NO level did not necessarily reflect regional or local NO availability, and that local NO production was modulated not only by NOS gene transcription but also by other mechanisms such as glycemic control, substrate for NOS availability, and endogenous NOS inhibitors (32). Nevertheless, the possibility that hyperglycemia-induced gut barrier dysfunction is caused by modulating NO bioavailability *in situ* cannot be excluded. As another regulatory factor in gut barrier function, previous studies indicated that TNF played a critical role in *in vivo* and *in vitro* experimental settings (12, 33). For examples, TNF-α caused the disruption of tight junction in intestinal epithelial cells by up-regulating myosin light chain kinase activity and expression (34), and gut barrier function in patients with Crohn's disease, characterized by permeable epithelial barrier, was restored by anti-TNF treatment using monoclonal antibody (12). In this experiment, we applied a TACE inhibitor which was found to have competitive properly against TACE *per se* to inhibit cleavage of membranous TNF-α and release soluble TNF-α, and found that an inhibition of TACE suppressed gut mucosal permeability significantly despite a marked hyperglycemia presented. Thus, soluble TNF-α was apparently engaged as a major factor in the regulation of gut barrier dysfunction induced by hyperglycemia in this endotoxemic animal. However, the present study was unable to answer whether the presence of membrane-bound TNF-α, characterized by potent protective property against lethal dose of LPS (35), or limited amount of soluble TNF-α is a key factor to minimize hyperglycemia-augmented gut barrier dysfunction. On the other hand, given the finding that IL-1β was also significantly discharged in group G as shown in Figure 2, IL-1β could be another contributor to the hyperglycemia-augmented gut barrier dysfunction. Indeed, recent study demonstrated that IL-1β increased gut epithelial tight junction permeability possibly through the activation of nuclear factor κB (36). Further study is warranted to examine the roles of IL-1β as well as biological activity of TACE in hyperglycemia-elicited gut barrier dysfunction.

There were several issues which should be resolved to justify our model. With a marked elevation of blood glucose, high serum osmolarity possibly caused by hyperglycemic state could modulate the outcome of this study. However, serum osmolarity calculated using a standard formula showed no significant differences between the groups (Table 1). Second, we applied low-dose endotoxin injection to mimic critically ill state. Under this dose of endotoxin injection with fluid therapy, mean arterial pressure remained constant and gut mucosal permeability was increased slightly but significantly at 3 hours in our pilot study. Some may argue that the range of hyperglycemia in this model might be too high to represent clinical situation. In our pilot study, we were unable to keep 200–300 mg/dL of blood glucose for 3- to 5-hour study period by using 10% or 20% glucose solution in this endotoxemic rat model possibly because of endogenous insulin discharges. Although the validity of clinical relevance in this hyperglycemia model may become lesser, we were obliged to choose 40% glucose solution in group G, and found the reproducibility of stable hyperglycemia and the similar extent of hyperinsulinemia to group GI in this experimental setting. Previous study using burned animal model also showed that a marked hyperglycemia, primarily intended to range between 250 and 350 mg/dL of blood glucose, reached approximately 300–450 mg/dL to be examined (15). It might be occasionally tough to keep this range of hyperglycemia for certain time periods in animal model of critically ill. Third, the 3-hour study period might be too short to be relevant to clinical situations that usually persist for several days. Indeed, we were unable to find significant alterations of gut microflora despite a marked increase of mucosal permeability. Chronic hyperglycemia enhanced production of reactive oxygen species accompanied by attenuation of

antioxidant mechanisms (37), whereas even short term of hyperglycemia could modulate immune function and cytokine production (6, 38). Ling et al (6) demonstrated that 3 hours of hyperglycemia (300–350 mg/dL) increased the discharges of inflammatory cytokines. On the contrary, the present study showed that only 3 hours, being rather realistic in clinical situation as an interval of blood glucose evaluation, was long enough to cause these significant alterations of gut mucosal permeability if excessive hyperglycemia persisted. Fourth, our study design may not allow us to answer the issue which factor, keeping normoglycemia vs. glycemia-independent action of insulin, was significant to ameliorate hyperglycemia-augmented gut barrier dysfunction in endotoxemia as previously reported (15). However, it should be noted that gut barrier function was apparently different between group G and GI, both of which showed the similar level of hyperinsulinemia. In other words, gut barrier dysfunction associated with hyperglycemia was restored, at least, independently of plasma insulin concentration. Finally, we applied an *in vivo* ligated intestinal loop model, characterized by anatomically intact blood supply and drainage as well as autonomic innervation, to evaluate gut mucosal permeability although several limitations were pointed out (39, 40).

In conclusion, hyperglycemia deteriorates endotoxin-induced gut barrier dysfunction which can be restored by keeping normoglycemia with insulin infusion. Among several factors, the modulation of soluble TNF-α discharges plays a significant role to prevent bacterial translocation in critically ill.

REFERENCES

1. Marik PE, Raghavan M: Stress-hyperglycemia, insulin and immunomodulation in sepsis. *Intensive Care Med* 2004; 30:748–756
2. Krinsley JS: Association between hyperglycemia and increased hospital mortality in a heterogenous population of critically ill patients. *Mayo Clin Proc* 2003; 78:1471–1478
3. Van den Berghe G, Wousters P, Weekwers F, et al: Intensive insulin therapy in critically ill patients. *N Engl J Med* 2001; 345:1359–1367
4. Van den Berghe G, Wilmer A, Hermans G, et al: Intensive insulin therapy in the medical ICU. *N Engl J Med* 2006; 354:449–461
5. Brunkhorst FM, Engel C, Bloos F, et al: Intensive insulin therapy and pentastarch resuscitation in severe sepsis. *N Engl J Med* 2008; 358:125–139
6. Ling PR, Smith RJ, Bistrian BR: Hyperglycemia enhances the cytokine production and oxidative responses to a low but not high dose of endotoxin in rats. *Crit Care Med* 2005; 33:1084–1089
7. Brix-Christensen V, Andersen SK, Andersen R, et al: Acute hyperinsulinemia restrains endotoxin-induced systemic inflammatory response: An experimental study in a porcine model. *Anesthesiology* 2004; 100:861–870
8. Van den Berghe G, Wousters P, Bouillon R, et al: Outcome benefit of intensive insulin therapy in the critically ill: Insulin dose versus glycemic control. *Crit Care Med* 2003; 31:359–366
9. Chen HI, Yeh DY, Liou HL, et al: Insulin attenuates endotoxin-induced acute lung injury in conscious rats. *Crit Care Med* 2006; 34:758–764
10. Meakins JL, Marshall JC: The gastrointestinal tract: The motor of multiple organ failure. *Arch Surg* 1986; 121:197–201
11. Kubes P: Nitric oxide modulates epithelial permeability in the feline small intestine. *Am J Physiol* 1992; 262:G1138–G1142
12. Suenaert P, Bulteel V, Lemmens L, et al: Anti-tumor necrosis factor treatment restores the gut barrier in Crohn's disease. *Am J Gastroenterol* 2002; 97:2000–2004
13. Esposito K, Nappo F, Marfella R, et al: Inflammatory cytokine concentrations are acutely increased by hyperglycemia in humans: Role of oxidative stress. *Circulation* 2002; 106:2067–2072
14. Bengmark S: Use of some pre-and pro- and synbiotics in critically ill patients. *Best Pract Res Clin Gastroenterol* 2003; 17:833–848
15. Ellger B, Debaveye Y, Vanhorebeek I, et al: Survival benefits of intensive insulin therapy in critical illness: Impact of maintaining normoglycemia versus glycemia-independent actions of insulin. *Diabetes* 2006; 55:1096–1105
16. Guo W, Magnotti L, Ding J, et al: Influence of gut microflora on mesenteric cytokine production in rats with hemorrhagic shock. *J Trauma* 2002; 52:1178–1185
17. Kosugi S, Morisaki H, Satoh T, et al: Epidural analgesia prevents endotoxin-induced gut mucosal injury in rabbits. *Anesth Analg* 2005; 101:265–272
18. Shimizu K, Ogura H, Asahara T, et al: Altered gut flora and environment in patients with severe SIRS. *J Trauma* 2006; 60:126–133
19. Jansen GJ, Wildeboer-Veloo AC, Tonk RH, et al: Development and validation of an automated, microscopy-based method for enumeration of groups of intestinal bacteria. *J Microbiol Methods* 1999; 37:215–221
20. Matsuda K, Tsuji H, Asahara T, et al: Sensitive quantitative detection of commensal bacteria by rRNA-targeted reverse transcription-PCR. *Appl Environ Microbiol* 2007; 73:32–39
21. Kikuchi H, Yajima T: Correlation between water-holding capacity of different types of cellulose in vitro and gastrointestinal retention time in vivo of rats. *J Sci Food Agr* 1992; 60:139–146
22. Suzuki T, Morisaki H, Serita R, et al: Infusion of the β-adrenergic blocker esmolol attenuates myocardial dysfunction in septic rats. *Crit Care Med* 2005; 33:2294–2301
23. Finney S, Zekveld C, Elia A, et al: Glucose control and mortality in critically ill patients. *JAMA* 2003; 290:2041–2047
24. Condon C, Squires C, Squires L: Control of rRNA transcription in *Escherichia coli*. *Microbiol Rev* 1995; 59:623–645
25. Macfarlane S, Macfarlane G: Regulation of short-chain fatty acid production. *Proc Nutr Soc* 2003; 62:67–72
26. Blottiere B, Buechaer B, Galmiche J, et al: Molecular analyses of the effect of short-chain fatty acids on intestinal cell proliferation. *Proc Nut Soc* 2003; 62:101–106
27. Fallingborg J: Intraluminal pH of the human gastrointestinal tract. *Dan Med Bull* 1999; 46:183–196
28. Schneider SM, Le Gall P, Girard-Popau F, et al: Total artificial nutrition is associated with major changes in the fecal flora. *Eur J Nutr* 2000; 39:248–255
29. Xu DZ, Lu Q, Deitch EA: Nitric oxide impairs intestinal barrier function. *Shock* 2002; 17: 139–145
30. Lamarque D, Whittle BJ: Increase in gastric intramucosal hydrogen ion concentrations following endotoxin challenge in the rat and the actions of nitric oxide synthase inhibitors. *Clin Exper Pharmacol Physiol* 2001; 28:164–168
31. Gomez-Jimenez J, Salgado A, Mourelle M, et al: L-arginine: Nitric oxide pathway in endotoxemia and human septic shock. *Crit Care Med* 1995; 23:253–258
32. Ellger B, Langouche L, Richir M, et al: Modulation of regional nitric oxide metabolism: Blood glucose control or insulin? *Intensive Care Med* 2008; 34:1525–1533
33. Zolotarevsky Y, Hecht G, Koutsouris A, et al: A membrane-permeant peptide that inhibits MLC kinase restores barrier function in vitro models of intestinal disease. *Gastroenterology* 2002; 123:163–172
34. Ye D, Ma I, Ma TY: Molecular mechanism of tumor necrosis factor—A modulation of intestinal epithelial tight junction barrier. *Am J Physiol* 2006; 290:G496–G504
35. Mohler KM, Sleath PR, Fitzner JN, et al: Protection against a lethal dose of endotoxin by an inhibitor of tumor necrosis factor processing. *Nature* 1994; 370:218–220
36. Al-Sadi RM, Ma TY. IL-1β causes an increase in intestinal epithelial tight junction permeability. *J Immunol* 2007; 178:4641–4649
37. Lelkes E, Unsworth BR, Lelkes PI: Reactive oxygen species, apoptosis and altered NGF-induced signaling in PCI2 pheochromocytome cells cultured in elevated glucose: An in vitro cellular model for diabetic neuropathy. *Neurotox Res* 2001; 3:189–203
38. Kwoun MO, Ling PR, Lydon E, et al: Immunologic effects of acute hyperglycemia in nondiabetic rats. *J Parenter Enteral Nutr* 1997; 21:91–95
39. Tagesson C, Sjodahl R, Thoren B: Passage of molecules through the wall of the gastrointestinal tract I. A simple experimental model. *Scand J Gastroenterol* 1978; 13:519–524
40. Otamiri T, Sjödahl R, Tagesson C: Lysophosphatidylcholine potentiates the increase in mucosal permeability after small-intestinal ischaemia. *Scand J Gastroenterol* 1986; 21:1131–1136

ブリーフレポート

鈴木康生[1]　加藤純悟[1]
藍　公明[1]　森山　潔[1]
志水秀行[2]　武田純三[1]
慶應義塾大学医学部麻酔学教室[1]
慶應義塾大学医学部外科学教室（心臓血管）[2]

ステントグラフト内挿術後の腹部大動脈瘤に対し人工血管置換術を施行した1例

<Brief Report>

Open Abdominal Aortic Aneurysm Repair after Endovascular Stent Grafting

Yasuo Suzuki[1], Jungo Kato[1],
Komei Ai[1], Kiyoshi Moriyama[1],
Hideyuki Shimizu[2] and Junzo Takeda[1]
Department of Anesthesiology[1],
Department of Cardiovascular Surgery[2],
School of Medicine, Keio University

An 87-year-old woman with interstitial pneumonia and renal dysfunction had persistent type II endoleak after endovascular stent grafting for abdominal aortic aneurysm (AAA). Four years after the stent grafting, she underwent open AAA repair under general anesthesia. The operation was successfully performed and the patient was discharged 2 weeks after the operation. Open AAA repair after stent grafting is expected to increase in the future, and anesthesiologists need to take account the risks not only arising from patients but also from surgical procedure.

(*J Clin Anesth (Jpn)* 2009；33：1049-50)

Key words：Endovascular stent grafting, Open abdominal aortic aneurysm repair, Endoleak

腹部大動脈瘤（abdominal aortic aneurysm：AAA）に対するステントグラフト手術は，欧米ではAAA治療の約50％を占め，本邦でも頻度は増加している[1]．大動脈ステントグラフト内挿術施行4年後に，人工血管置換術を施行した症例を経験した．

症　例

87歳の女性．身長153 cm，体重41 kg．1歳時に腎膿瘍で左腎を摘出した．間質性肺炎を合併していたため，83歳時にAAAに対しY型ステントグラフト内挿術を施行した．術後3カ月頃よりendoleak type IIを疑われ外来で経過観察していたが，瘤の増大傾向を認め今回開腹手術を予定した．

キーワード：ステントグラフト，人工血管置換術，エンドリーク

術前検査でクレアチニンクリアランスは52 mL/minと低下し，胸部X線写真で両側肺野の透過性が低下していた．Hugh-Jones分類はI度で，呼吸機能検査で1秒率76％，1秒量1.21 Lと閉塞性肺障害を認めた．心電図で完全右脚ブロック，左脚前枝ブロックを認めたが，経胸壁心エコーで心機能は良好とされた．

腹部CT検査では，腎動脈分岐後約1.5 cmにステントグラフトの上端が存在し，瘤の最大径は63×53 mm，腰動脈からendoleakが疑われた（Fig. 1）．開腹してのYグラフト置換術を予定したが，瘤周囲の癒着，大動脈遮断が腎動脈分岐部より中枢側になる可能性，術野でステントグラフトの位置確認に難渋する可能性，血管内膜損傷の可能性など，手術操作が困難となることが予想された．

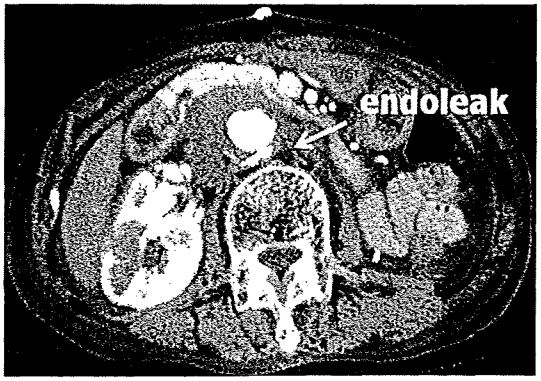

Fig. 1　Type II endoleak from lumbar artery.

麻酔はプロポフォール＋レミフェンタニルによる静脈麻酔に硬膜外麻酔を併用し，心拍出量モニタリングのためフロートラックセンサー®およびプリセップカテーテル®を用いた．心係数および中心静脈血酸素飽和度は術中から術後1日まで計測された．瘤周囲の

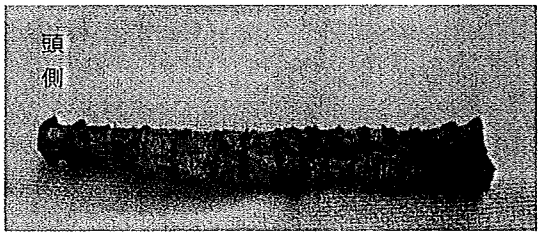

Fig. 2 Type II endoleak from lumbar artery.

癒着剝離は容易で，大動脈遮断はステントグラフトを含めず腎動脈分岐下で可能であった．瘤を切開したところ腰動脈からの血液流入を認めた．ステントグラフトは無事摘出され（Fig. 2），同部位にＹ型人工血管を留置した．手術時間は4時間，麻酔時間は5時間35分で，出血量は1,500 mL，尿量は700 mL，輸液量は6,050 mL，輸血量は780 mL，自己回収血輸血は750 mLであった．術中循環動態は安定し，手術室内で抜管後集中治療室へ入室した．心係数は術中1.9～2.8 L/min/m²，術後2.8～3.3 L/min/m²，中心静脈血酸素飽和度は術中71～90%，術後73～83%に保たれた．術後経過は良好で2週間後に退院した．

考　　察

AAAに対するステントグラフトを用いた治療は，本邦では2002年にステントグラフト内挿術として保険適用となり，2006年よりZenith AAA endovascular graft（Cook社）が治療用デバイスとして保険適用となった．本邦での使用頻度は上昇しており，AAA治療全体の40%を占める見込みである[1]．ステントグラフト内挿術の術後に1.8～28%で人工血管置換術が必要になるとの報告があり[2-4]，endoleak，endotension，migration，graft disconnectionにより大動脈瘤の破裂をきたした報告もある[5]．本邦でもステントグラフト術後の人工血管置換術に関しての報告が散見される[6-9]．

ステントグラフト内挿術後の人工血管置換術は，患者の術前リスクが高いことに加え，手術操作自体が難航することがある[6]．本症例でも，患者は高齢な上に腎機能および肺機能が低下しており，また，手術が難航する可能性が考えられた．ステントグラフト抜去時には，内膜損傷・大動脈解離や血栓塞栓症により血栓除去，腎動脈再建，下肢バイパス術などの追加手術が必要となるとの報告がある[2]．ステントグラフト挿入術の術中術後に種々の理由で緊急人工血管置換術が必要となった症例では，多臓器不全，心合併症，呼吸器不全による死亡率が高いことが報告されている[3]．

本邦で今後，ステントグラフト後のAAAに対する開腹術が増加すると思われる．その際は患者の術前リスクが高く，手術も難航する可能性が高いため，麻酔科医も術前からその対策を検討する必要がある．

文　献

1) 四津良平，石丸　新，加藤雅明，他：大動脈ステントグラフト内挿術の合併症とその対策．CIRCULATION Up-to-Date 2008；3：352-61
2) Tiesenhausen K, Hessinger M, Konstantiniuk P, et al: Surgical conversion of abdominal aortic stent-grafts. Eur J Vasc Endovasc Surg 2006；31：36-41
3) Cuypers PWM, Laheij RJF, Buth J, et al: Which factors increase the risk of conversion to open surgery following endovascular abdominal aortic aneurysm repair? Eur J Vasc Endovasc Surg 2000；20：183-89
4) Biebl M, Hakaim A, Oldenburg W, et al: Midterm results of a single-center experience with commercially available devices for endovascular aneurysm repair. Mt Sinai J Med 2005；72：127-35
5) Schlösser FJ, Gusberg RJ, Dardik A, et al: Aneurysm rupture after EVAR. Eur J Vasc Endovasc Surg 2009；37-1：15-22
6) 伊藤寿朗，川原田修義，栗本義彦，他：腹部大動脈瘤ステントグラフト内挿術後同部位に人工血管置換術を施行した2例．日心外会誌 2007；36：141-4
7) 渡部芳子，石丸　新，川口　聡，他：ステントグラフト内挿術後の人工血管置換術に工夫を要した腹部大動脈瘤の1例．日血外会誌 2005；14：14-34
8) 一関一行，伊東和雄，棟方　護，他：ステントグラフト内挿術後再破裂をきたした破裂性動脈瘤の2例．日心外会誌 2007；33：34-7
9) 秋田淳年，栃井将人，星野　竜，他：ステントグラフト治療5年後の破裂に対して外科手術で救命し得た腹部大動脈瘤の1例．日血外会誌 2007；16：55-8

*　　*　　*

Can Mixed Venous Hemoglobin Oxygen Saturation Be Estimated Using a NICO Monitor?

Yoshifumi Kotake, MD, PhD*

Takashige Yamada, MD†

Hiromasa Nagata, MD†

Takeshi Suzuki, MD, PhD†

Junzo Takeda, MD, PhD†

BACKGROUND: We hypothesized that mixed venous hemoglobin oxygen saturation (SvO_2) can be estimated by calculation from CO_2 production, cardiac output, and arterial oxygen saturation measured using a noninvasive cardiac output (NICO) monitor (Novametrix-Respironics, Wallingford, CT).

METHODS: Twenty-three patients undergoing aortic aneurysm repair underwent SvO_2 monitoring using a pulmonary artery catheter and cardiac output monitoring using a NICO monitor. The estimated SvO_2 value calculated from NICO monitor-derived values was compared with the SvO_2 value measured using a pulmonary artery catheter. The accuracy of this estimation was analyzed with Bland-Altman method. The ability of this estimation to track the change of SvO_2 was also evaluated using correlation analysis to compare the changes of estimated SvO_2 and measured SvO_2.

RESULTS: The bias ± limits of agreement of the estimated SvO_2 against measured SvO_2 was −2.1% ± 11.2%. The change of estimated SvO_2 was modestly correlated with the change of measured SvO_2.

CONCLUSIONS: SvO_2 derived from the values measured by the NICO monitor cannot be used interchangeably with the values measured spectrophotometrically using the pulmonary artery catheter. More refinement is required to obtain more reliable estimate of SvO_2 less invasively. However, large changes of SvO_2 may be detected with this method and can be used as a precautionary sign when the balance between oxygen supply and demand is compromised without inserting a central venous catheter.

(Anesth Analg 2009;109:119-23)

Mixed venous oxygen saturation (SvO_2) or its surrogate, central venous oxygen saturation ($ScvO_2$), is used to assess the oxygen supply-demand relationship.[1–3] However, central venous access is required to measure these values, which carries some risk to the patient. Theoretically, SvO_2 can be calculated using cardiac output (CO), the concentration of oxygen saturated hemoglobin (Hb), and oxygen consumption (VO_2).[4] If the relationship between VO_2 and CO_2 production (VCO_2) remains stable during anesthesia, SvO_2 can be estimated with CO, VCO_2, and Hb concentration and its arterial oxygen saturation. Because CO, VCO_2, and Spo_2 are continuously monitored with a noninvasive cardiac output (NICO) monitor (Respironics-Novametrics, Wallingford, CT), we hypothesized that SvO_2 could be mathematically estimated using these NICO-derived parameters and the Hb concentration.[5,6] The purpose of this prospective study was to assess the accuracy of estimating SvO_2 using the NICO monitor in anesthetized, ventilated patients.

METHODS

The study protocol was approved by the IRB of Keio University, and written informed consent was obtained from the participants. Twenty-three patients undergoing elective infrarenal aortic reconstruction were enrolled in this prospective, observational study. Patients' lungs were mechanically ventilated with a tidal volume of 10 mL/kg, and the respiratory rate was adjusted to maintain normocapnia. CO, VCO_2, and Spo_2 were continuously monitored with a NICO monitor (Ver. 5.2, Novametrix-Respironics, Wallingford, CT). The NICO sensor was placed between the heat and moisture exchanger and the Y-piece of the respiratory circuit, and the length of the rebreathing circuit was adjusted to maintain optimal condition. NICO-derived CO, VCO_2, and Spo_2 values were downloaded to a personal computer and later used for calculation. For CO, results of average mode (CO-a)

From the *Department of Anesthesiology, Toho University Medical Center Ohmori Hospital; and †Department of Anesthesiology, School of Medicine, Keio University, Tokyo, Japan.

Accepted for publication January 21, 2009.

Supported by Intramural Department Sources Only.

Yoshifumi Kotake is a paid consultant of Edwards Lifesciences. All others authors have no conflict of interest to disclose.

Reprints will not be available from the author.

Address correspondence to Yoshifumi Kotake, MD, PhD, Department of Anesthesiology, Toho University Medical Center Ohmori Hospital, 6-11-1, Ohmori-nishi, Ohta, Tokyo 143-8541, Japan. Address e-mail to ykotake@med.toho-u.ac.jp.

DOI: 10.1213/ane.0b013e3181a85c22

were used. An 8Fr pulmonary artery catheter (PAC) equipped with continuous CO measurement and venous oximetry functions (746HF8, Edwards Lifesciences, Irvine, CA) was inserted via the right internal jugular vein. CO and SvO_2 were continuously monitored after the SvO_2 was calibrated using an *in vivo* method of measuring mixed venous blood with a CO-oximeter (Stat M Profile, Nova Biochemicals, Waltham, MA). The averaged SvO_2 during a 3-min rebreathing cycle of the NICO monitor was used as a representative measured SvO_2 value. Hb was measured every 60 min by the same blood gas analyzer. Between these measurements, Hb concentration was assumed to change linearly between these measurements, and these interpolated values were used for subsequent calculations.

Estimated SvO_2 is defined by following formula (see appendix):

$$\text{Estimated } SvO_2 = SpO_2 - \frac{VCO_2\,(mL/min)/0.85}{1.36 \times Hb\,(g/dL) \times CO\text{-}a\,(L/min) \times 0.1}$$

Data were excluded from the analysis when the signal quality indicator was reported as 3 or 4 by the Vigilance II monitor. Data obtained during the first 20 min after cross-clamp release were also excluded from the analysis, because venous blood returned from infrarenal lesions upon the release of cross-clamp was significantly hypoxemic and caused independent effects on SvO_2. Additionally, CO was measured several times during the surgery with intermittent bolus thermodilution method (ICO). The estimated SvO_2 value with ICO was then calculated by substituting the ICO value in the above formula to analyze the possible contribution of measurement error with NICO-derived CO.

Data are expressed as mean ± SD and were statistically analyzed using the Prism software (ver 4, Graphpad, San Diego, CA). Bland-Altman analysis was initially applied to the individual data to describe the agreement between estimated SvO_2 and measured SvO_2. Thereafter, the data were pooled to derive overall bias ± limits of agreement (2SD of difference) in all the measurement pairs. A correction was made according to the literature because multiple observations from individuals were used in this analysis.[7,8] To assess how the estimated SvO_2 tracks the changes of measured SvO_2, the relationship between the change of estimated SvO_2 between the two consecutive measurement against the incidental change of measured SvO_2 was analyzed with Pearson's correlation coefficient and regression analysis according to a previous report.[9]

RESULTS

Twenty male and three female patients participated in this study. The age, height, and weight of these participants were 72 ± 8 yr old, 164 ± 6 cm, and 62 ± 13 kg, respectively. The duration of surgery and of cross-clamp were 266 ± 54 min and 59 ± 18 min, respectively. The mean (range) of measured SvO_2 was 78% (44%–94%). One thousand three hundred thirty-three pairs of estimated SvO_2 and measured SvO_2 were included in the analysis. Between 45 and 82 pairs of measurements from each individual were included. The bias and the limits of agreement in each study subjects are summarized in Figures 1 and 2. Figure 3 demonstrates the Bland-Altman plot of all the measurements. The bias ± limits of agreement of estimated SvO_2 by NICO monitor was −2.1% ± 11.2% against the spectrophotometrically measured SvO_2. Even when the analysis was limited to the hemodynamically stable period, which is arbitrarily defined as CO change was within 2% between 3-min interval, the bias did not significantly change (1172 data points,

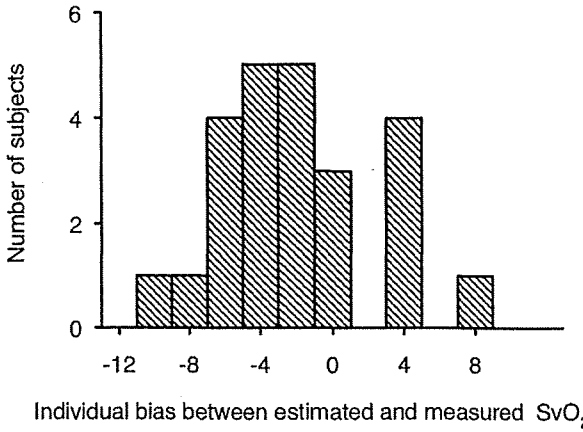

Figure 1. Distribution of bias between estimated mixed venous hemoglobin oxygen saturation (SvO_2) and measured SvO_2 from an individual subject. *x* axis denotes ranges of the bias from an individual subject. *y* axis denotes number of subjects. Number of the measurement in each subject varies between 45 and 82.

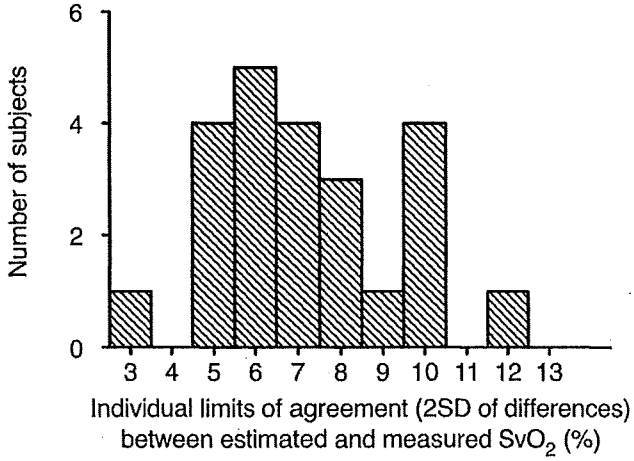

Figure 2. Distribution of precision between estimated mixed venous hemoglobin oxygen saturation (SvO_2) and measured SvO_2 from an individual subject. *x* axis denotes ranges of the limits of agreement from an individual subject. *y* axis denotes number of subjects. Number of the measurement in each subject varies between 45 and 82.

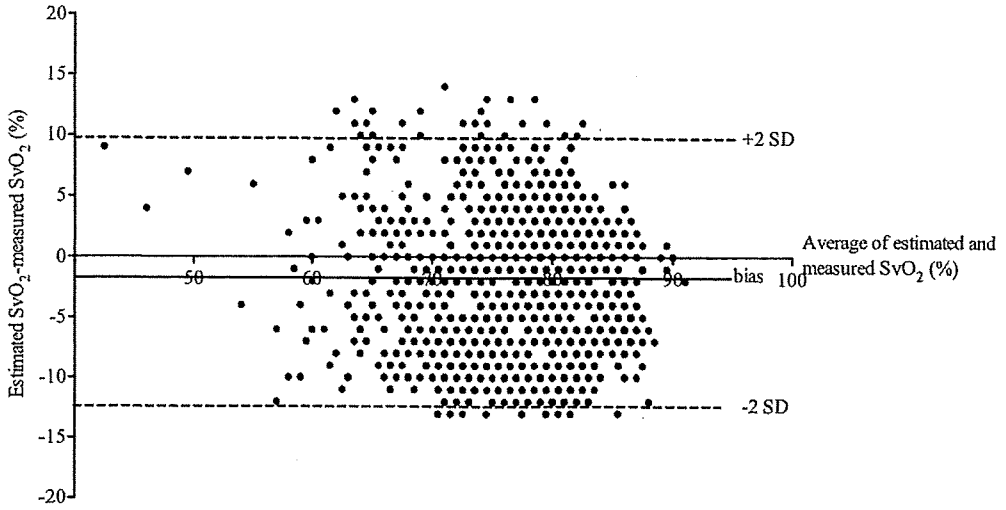

Figure 3. Bland-Altman plot of 1333 pairs of estimated and measured mixed venous hemoglobin oxygen saturation (SvO_2). The bias is demonstrated as a solid line, and the limits of agreement (2SD of the difference) are also demonstrated as a dashed line in this figure.

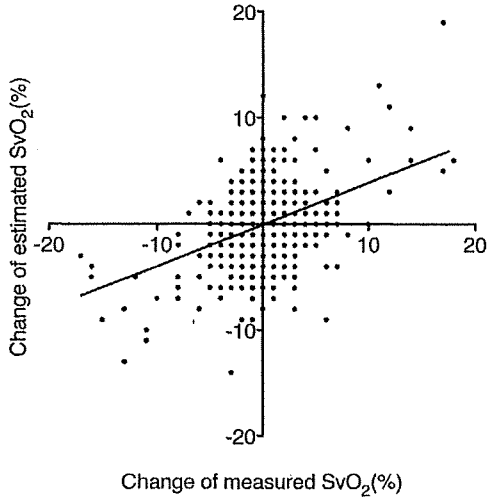

Figure 4. Changes of measured mixed venous hemoglobin oxygen saturation (SvO_2) and estimated SvO_2 between two consecutive measurement cycles. $n = 1265$, solid line denotes regression line: $r^2 = 0.145$, $P < 0.001$, the change of estimated $SvO_2 = 0.39 \times$ the change of measured $SvO_2 - 0.06$.

bias ± limits of agreement: −2.1% ± 11.0%). CO was determined with bolus thermodilution 120 times in these subjects. The bias ± limits of agreement of ICO-derived SvO_2 estimation against measured SvO_2 was −4.4% ± 13.8% and no clear improvement of agreement was demonstrated. The relationship between the change of estimated SvO_2 and the change of measured SvO_2 is summarized in Figure 4. The change of estimated SvO_2 was modestly but significantly correlated with the change of measured SvO_2 between the measurement cycle ($r^2 = 0.145$, $P < 0.001$).

DISCUSSION

This study demonstrated that the bias ± limits of agreement between the estimated SvO_2 and the measured SvO_2 were −2.1% ± 11.2%. This study confirmed that SvO_2 could be reasonably estimated by the NICO-derived parameters with several assumptions. However, these data indicate that the NICO-derived SvO_2 value cannot be used interchangeably against the SvO_2 value obtained with PAC equipped with oximetry function.

It is intuitively advantageous to objectively assess hemodynamic status with CO. However, the goal of hemodynamic optimization should be to achieve well-balanced oxygen supply and VO_2 instead of a predetermined CO. Based on this perspective, the clinical importance of venous oximetry as a tool to evaluate oxygen supply-demand balance is well established.[1,2] However, measuring SvO_2 requires PAC insertion, which carries some additional risk over central venous catheterization. Alternatively, $ScvO_2$ has been used for the same purpose.[3,10] However, previous reports demonstrated that there was a significant variability between SvO_2 and $ScvO_2$ and concluded that these two parameters are not interchangeable.[9,11–13] The differences in regional oxygen extraction, especially the hepatosplanchnic region and central nervous system have been attributed to this significant variability. To assess the balance of oxygen supply and demand less invasively, several attempts have been made to estimate the SvO_2 value without inserting a central venous catheter.[14–16] Alternatively, SvO_2 can be estimated if CO, Hb, SaO_2, and VO_2 are known. As NICO measures CO, SpO_2, and VCO_2, we speculated that SvO_2 could be calculated with reasonable accuracy if Hb and the relationship between VO_2 and VCO_2 were adequately estimated.

We found considerably wide limits of agreement between the estimated SvO_2 and the measured SvO_2. This finding may be attributed to several factors, including the inaccuracy or the temporal delay of one of the measured values incorporated into the formula and several assumptions. First, the accuracy of CO measurement may contribute to a relatively large variation. The NICO monitor has been known to